THE JOURNAL OF BIOLOGICAL CHEMISTRY VOL. 291, NO. 9, pp. 4826–4843, February 26, 2016

Identification of Glycosylation Sites Essential for Surface Expression of the $Ca_V\alpha2\delta1$ Subunit and Modulation of the Cardiac $Ca_V1.2$ Channel Activity*

Received for publication, September 13, 2015, and in revised form, January 6, 2016 Published, JBC Papers in Press, January 7, 2016, DOI 10.1074/jbc.M115.692178

Marie-Philippe Tétreault[‡1], Benoîte Bourdin[‡1], Julie Briot[‡], Emilie Segura[‡], Sylvie Lesage[§], Céline Fiset[¶], and Lucie Parent[‡2]

From the [‡]Département de Physiologie Moléculaire et Intégrative, Faculté de Médecine, and [¶]Faculté de Pharmacie, Institut de Cardiologie de Montréal and [§]Département de Microbiologie, Infectiologie, and Immunologie, Faculté de Médecine, Centre de Recherche de l'Hôpital Maisonneuve-Rosemont, Université de Montréal, Montréal, Québec H3C 3J7, Canada

Alteration in the L-type current density is one aspect of the electrical remodeling observed in patients suffering from cardiac arrhythmias. Changes in channel function could result from variations in the protein biogenesis, stability, post-translational modification, and/or trafficking in any of the regulatory subunits forming cardiac L-type Ca^{2+} channel complexes. $Ca_V\alpha2\delta1$ is potentially the most heavily *N*-glycosylated subunit in the cardiac L-type $Ca_V1.2$ channel complex. Here, we show that enzymatic removal of *N*-glycans produced a 50-kDa shift in the mobility of cardiac and recombinant $Ca_V\alpha2\delta1$ proteins. This change was also observed upon simultaneous mutation of the 16 Asn sites. Nonetheless, the mutation of only 6/16 sites was sufficient to significantly 1) reduce the steady-state cell surface fluorescence of $Ca_V\alpha2\delta1$ as characterized by two-color flow cytometry assays and confocal imaging; 2) decrease protein stability estimated from cycloheximide chase assays; and 3) prevent the $Ca_V\alpha2\delta1$-mediated increase in the peak current density and voltage-dependent gating of $Ca_V1.2$. Reversing the N348Q and N812Q mutations in the non-operational sextuplet Asn mutant protein partially restored $Ca_V\alpha2\delta1$ function. Single mutation N663Q and double mutations N348Q/N468Q, N348Q/N812Q, and N468Q/N812Q decreased protein stability/synthesis and nearly abolished steady-state cell surface density of $Ca_V\alpha2\delta1$ as well as the $Ca_V\alpha2\delta1$-induced up-regulation of L-type currents. These results demonstrate that Asn-663 and to a lesser extent Asn-348, Asn-468, and Asn-812 contribute to protein stability/synthesis of $Ca_V\alpha2\delta1$, and furthermore that *N*-glycosylation of $Ca_V\alpha2\delta1$ is essential to produce functional L-type Ca^{2+} channels.

The regulation of Ca^{2+} influx in cardiac cells is critical to the generation of the force necessary for the myocardium to meet the physiological needs of the body (1). In resting cells, intracellular free ionized Ca^{2+} is maintained at a low concentration (high nanomolar range) by the concerted action of mechanisms that prevent Ca^{2+} entry, promote its extrusion (mostly via the Na^+/Ca^{2+} exchanger), and ensure its storage in the sarcoplasmic reticulum (2). Ca^{2+} entry is mediated mainly by the cardiac L-type Ca^{2+} channel, which is central to the initiation of excitation-contraction coupling via Ca^{2+}-induced Ca^{2+} release from the sarcoplasmic reticulum. Regulation of the L-type Ca^{2+} current has profound physiological significance. Indeed, alterations in density or the activation/inactivation gating of L-type Ca^{2+} channels have been implicated in a variety of cardiovascular diseases (3, 4), including cardiac arrhythmias such as atrial fibrillation (5–8), heart failure (9, 10), and ischemic heart disease (10). The molecular mechanisms underlying changes in the activity of the L-type Ca^{2+} channel remain under study for most pathologies.

The L-type $Ca_V1.2$ channel belongs to the molecular family of high voltage-activated Ca_V channels. High voltage-activated $Ca_V1.2$ channels are hetero-oligomers composed of the main pore-forming $Ca_V\alpha1$ subunit non-covalently bound to the cytoplasmic $Ca_V\beta$ auxiliary subunit, the EF-hand protein calmodulin (constitutively bound to the C terminus of $Ca_V\alpha1$), and the $Ca_V\alpha2\delta$ subunit (11–16). The full complement of auxiliary subunits is required to produce high voltage-activated $Ca_V1.2$ channels with the properties of the native channels. $Ca_V\beta$ promotes the cell surface density of $Ca_V1.2$ channels through a high affinity interaction (17) in part by preventing its degradation by the ubiquitin/proteasome system (18). Co-expression of the $Ca_V\alpha2\delta$ subunit with $Ca_V\beta$-bound $Ca_V\alpha1$ increases peak current density and promotes channel activation at more negative voltages (19–23). Although the molecular mechanism underlying this effect remains to be fully elucidated, the cell surface density of $Ca_V\alpha2\delta1$ dictates the net Ca^{2+} influx through L-type Ca^{2+} channels (22). The $Ca_V\alpha2\delta1$ subunit, encoded by *CACNA2D1*, is expressed in skeletal muscle (24) and in cardiac muscle (25) where it is the main isoform associated with $Ca_V1.2$ (25, 26). The $Ca_V\alpha2\delta$ proteins undergo complex co- and post-translational modifications. Endogenous $Ca_V\alpha2$ and $Ca_V\delta$ are usually thought to be produced as a single protein that is proteolytically cleaved and then linked through strong disulfide bonds (27, 28). Although $Ca_V\alpha2\delta$ has been traditionally described as a type I transmembrane protein, it has been recently shown that $Ca_V\alpha2\delta$ proteins associate with the plasma membrane through a glycosylphosphatidylinositol

* This work was supported by Canadian Institutes of Health Research Operating Grant 130256 and a grant-in-aid from the Heart and Stroke Foundation of Canada (to L. P.). The authors declare that they have no conflicts of interest with the contents of this article.
[1] Both authors contributed equally to this work.
[2] To whom correspondence should be addressed: Département de Physiologie Moléculaire et Intégrative, Université de Montréal, P. O. Box 6128, Downtown Station, Montréal, Quebec H3C 3J7, Canada. Tel.: 514-343-6673; E-mail: lucie.parent@umontreal.ca.

anchor attached to $Ca_V\delta$ (29), although the functional relevance of this process remains to be fully established (30). $Ca_V\alpha2\delta$ subunits are also heavily glycosylated. It is estimated that *N*-glycans contribute as much as ≈30–50 kDa to the molecular mass of $Ca_V\alpha2\delta1$ (26, 27, 31, 32) making it a unique target for endoplasmic reticulum (ER)[3] glycoprotein quality control (33–36).

Glycosylation is a form of co- and post-translational covalent modification that serves a variety of structural and functional roles in membrane and secreted proteins. The major classes of glycans being produced in eukaryotic cells are as follows: 1) Asn (*N*)-linked glycans attached to the nitrogen atom of asparagine side chains; 2) *O*-linked glycans attached to the hydroxyl oxygen of serine, threonine, tyrosine, hydroxylysine, or hydroxyproline side chains; and 3) *C*-linked glycans, a rare form of glycosylation, attached to a carbon on a tryptophan side chain. *N*-Glycosylation, one of the most abundant types of protein glycosylation (37), is initiated by the co-translational addition by the oligosaccharyltransferase of glucose$_3$-mannose$_9$-*N*-acetylglucosamine$_2$ core oligosaccharides to the Asn residue of the lumenally exposed consensus glycosylation site Asn-Xaa-(Ser/Thr) (N*X*(S/T)) where Xaa is any amino acid except proline (Pro), serine (Ser), and threonine (Thr) (38). The transfer of *N*-glycans to Asn-Xaa-(Ser/Thr) sites occurs on the lumenal side of the ER membrane while the protein moiety is being synthesized on ER-bound ribosomes; hence, only domains that are accessible to the ER lumen will receive *N*-glycans. Membrane glycoproteins remain anchored in the ER membrane with portion(s) either exposed to the ER lumen, embedded in the membrane, or within the cytoplasm. Subsequent trimming of glucose and mannose residues determines whether the polypeptide undergoes additional folding cycles or is targeted for the ER-associated degradation (ERAD) by retrotranslocation and ubiquitin proteasome-dependent proteolysis in the cytosol. This process is critical for protein biosynthesis, and abrogation of glycosylation causes embryonic lethality in mice (39).

Defective glycosylation of cardiac ion channels plays a role in multiple cardiac pathologies (40–44). In this work, we have characterized the role of *N*-glycosylation on cell surface density and the function of the $Ca_V\alpha2\delta1$ auxiliary subunit using mobility shift assays, cycloheximide pulse-chase analysis, confocal imaging, flow cytometry assays, and patch clamp recordings of recombinant $Ca_V1.2$ currents. Here, we showed that a single mutation at Asn-663 prevented the cell surface presentation and the function of $Ca_V\alpha2\delta1$, although the protein remains strongly glycosylated. Mutations of other sites proved to alter channel function to a lesser extent. Simultaneous mutation of 6/16 consensus *N*-glycosylation sites in the extracellular portion of the $Ca_V\alpha2\delta1$ protein curtailed protein stability and impaired channel function with a predominant role for Asn-348 and Asn-812. Furthermore, combining the N468Q mutation with N348Q and/or N812Q disturbed L-type channel function. Single mutations of the other Asn sites (out of the 16 tested) were without significant functional impact. Altogether, our data support a model where four Asn residues are essential to form functional L-type $Ca_V1.2$ currents.

Experimental Procedures

Recombinant DNA Techniques—The rabbit $Ca_V1.2$ (GenBank™ accession number X15539) and the rat $Ca_V\beta3$ (GenBank™ accession number M88751) (45) were subcloned in commercial vectors under the control of the CMV promoter as described elsewhere (22, 46). The primary sequence (1091 residues) of the rat brain $Ca_V\alpha2\delta1$ clone (GenBank™ accession number NM_012919) (47) was subcloned in three vectors. Most experiments were performed with pmCherry-$Ca_V\alpha2\delta1$-HA, where $Ca_V\alpha2\delta1$ was subcloned in the pmCherry-N1 vector (Cederlane, Burlington, Ontario, Canada) between the SacI and SalI sites, and the hemagglutinin (HA) epitope (YPYDVPDYA) was inserted in the extracellular domain of $Ca_V\alpha2$ between Asp-676 and Arg-677 (22). $Ca_V\alpha2\delta1$ was also subcloned in homemade vectors derived from the pCMV-Script vector and are referred to as pCMV-$Ca_V\alpha2\delta1$ and pC2-$Ca_V\alpha2\delta1$ in Fig. 2*B*. Except for Fig. 2*B*, the pmCherry-$Ca_V\alpha2\delta1$-HA construct was used throughout.

Site-directed Mutagenesis—Single pmCherry-$Ca_V\alpha2\delta1$-HA mutants were produced with the Q5 site-directed mutagenesis kit (New England Biolabs Inc., Whitby, Ontario, Canada) as described elsewhere (22). Multiple glycosylation mutations were introduced simultaneously in the pmCherry-$Ca_V\alpha2\delta1$-HA construct using Gibson Assembly Master Mix (New England Biolabs) according to the manufacturer's instructions. Briefly, multiple overlapping primers were designed to incorporate mutations in $Ca_V\alpha2\delta1$. Fragments containing the mutations were PCR-amplified, purified from agarose gel using QIAquick gel extraction kit (Qiagen, Mississauga, Ontario, Canada), and assembled with the 2× Gibson Assembly Master Mix before transformation into high efficiency DH5-α competent *Escherichia coli*. Constructs were verified by automated double-stranded sequence analysis (Genomics Platform, IRIC, Université de Montréal, Québec, Canada). In this work, multiple mutations are referred to as "yxNQ" where "y" denotes the number of Asn (N) to Gln (Q) or NQ mutations introduced in the constructs. Accordingly the multiple mutations used include: 4xNQ, N92Q/N348Q/N594Q/N876Q; 5xNQ, N92Q/N184Q/N468Q/N876Q/N986Q; 6xNQ, N92Q/N184Q/N348Q/N594Q/N812Q/N876Q; 7xNQ, N92Q/N184Q/N348Q/N594Q/N812Q/N876Q/N986Q; 13xNQ, N92Q/N136Q/N184Q/N348Q/N468Q/N585Q/N594Q/N769Q/N812Q/N876Q/N883Q/N986Q/N1066Q; 14xNQ, N92Q/N136Q/N184Q/N348Q/N468Q/N585Q/N594Q/N663Q/N769Q/N812Q/N876Q/N883Q/N986Q/N1066Q; and 16xNQ, N92Q/N136Q/N184Q/N324Q/N348Q/N468Q/N475Q/N585Q/N594Q/N663Q/N769Q/N812Q/N876Q/N883Q/N973Q/N986Q. Protein expression of these constructs was confirmed by Western blotting in total cell lysates as described previously (17, 22).

Cell Culture and Transfections—HEK293T or HEKT (human embryonic kidney 293 cells stably expressing an SV40 temperature-sensitive T antigen) and HEKT cells stably transfected with $Ca_V\beta3$ were grown in Dulbecco's high glucose minimum essential medium (DMEM-HG) supplemented with 10% fetal

[3] The abbreviations used are: ER, endoplasmic reticulum; ERAD, ER-associated degradation; PNGase F, peptide-*N*-glycosidase F; WGA, wheat germ agglutinin; pF, picofarad.

bovine serum, 1% penicillin/streptomycin at 37 °C under a 5% CO_2 atmosphere as described elsewhere (17, 22). HEKT cells were transfected at 80–90% confluence (1 million cells per 35-mm culture dish) with similar amounts of DNA (1:1 ratio or 4:4 μg) for pCMV-Ca_V1.2 WT and pCMV-based $Ca_V\alpha2\delta1$ constructs in 10 μl of Lipofectamine 2000 (Life Technologies, Inc.) using a DNA/lipid ratio of 1:2.5 (17, 22). The pmCherry-$Ca_V\alpha2\delta1$-HA construct was either expressed as pmCherry-$Ca_V\alpha2\delta1$-HA WT or as pmCherry-$Ca_V\alpha2\delta1$-HA NQ mutants. Mock transfection was achieved with the empty vector referred to as pmCherry-no insert. A total of 8 μg of DNA was thus transfected per 10^6 HEKT-stable $Ca_V\beta3$ cells in all experiments.

Culture and Imaging of Mouse Cardiomyocytes—Experiments were approved by the Animal Protection Committee of the Montreal Heart Institute (protocol 2014-44-01) and were performed in accordance with the guidelines of the Canadian Council for Animal Care and the Guide for the Care and Use of Laboratory Animals 8th Edition (2011). Ventricular myocytes were isolated from neonate (22, 48, 49) or adult (50) CD-1 mice as described elsewhere. In the latter case, CD-1 male mice (5 months old) (Charles River Laboratories, St. Constant, Canada) were anesthetized with isoflurane. Hearts were quickly removed and placed on ice-cold Tyrode's solution containing 130 mM NaCl, 5.4 mM KCl, 1 mM MgCl, 0.33 mM Na_2HPO_4, 10 mM HEPES, 5.5 mM glucose, and 1 mM $CaCl_2$, pH 7.4. Ventricles were isolated and homogenized at 4 °C in a Tris-based solution containing a mix of protease inhibitors (Sigma), including 4-(2-aminoethyl) benzenesulfonyl fluoride hydrochloride, aprotinin, bestatin, E-64, leupeptin, and 1 mM EDTA, pH 7.4 (50). Cells were fixed (2% paraformaldehyde, pH 7.4, 15 min, 4 °C), blocked, and permeabilized (2% normal donkey serum, 0.1% Triton X-100, 60 min, at room temperature). Three washes with phosphate-buffered saline (PBS) followed each step. After overnight incubation at 4 °C with primary anti-$Ca_V\alpha2\delta1$ antibody (1:50) (Santa Cruz Biotechnology) in 1% donkey serum with 0.05% Triton X-100, cells were incubated with the secondary Alexa 488 antibody (Life Technologies, Inc.) (1:800) for 90 min at room temperature. Cells were stained with DAPI (1:1000) (Life Technologies, Inc.) for 10 min to identify the nucleus and with the wheat germ agglutinin-647 (WGA-647) (1:200) (Life Technologies, Inc.) to visualize cell membrane glycoproteins (51, 52). WGA is a carbohydrate-binding protein of approximately 36 kDa that selectively recognizes sialic acid and *N*-acetylglucosaminyl sugar residues. Confocal fluorescent images were captured with a Zeiss LSM 710 confocal microscope system with a ×63/1.40 oil objective. The images were analyzed using FIJI software to delete background, subtract noise, and to produce co-localization pixel maps.

Live Imaging of HEKT Cells—HEKT cells stably transfected with $Ca_V\beta3$ were transiently transfected simultaneously with pCMV-Ca_V1.2 and pmCherry-$Ca_V\alpha2\delta1$-HA WT or NQ mutants. Cells were dissociated and seeded 6 h after transfection to obtain isolated cells for imaging. Exactly 24 h after transfection, cells were stained with the fluorescein isothiocyanate (FITC)-conjugated mouse monoclonal anti-HA. Nuclei were stained with DAPI (1:1000) (Life Technologies, Inc.) in 1× PBS for 45 min at 4 °C. Confocal fluorescent images were captured with the same Zeiss LSM 710 confocal microscope used for cardiomyocyte imaging (see above).

Glycosidase Assays—Isolated mouse cardiomyocytes or transfected HEKT cells were solubilized in a radioimmunoprecipitation assay (RIPA) buffer (150 mM NaCl, 1.0% IGEPAL® CA-630, 0.5% sodium deoxycholate, 0.1% SDS, and 50 mM Tris, pH 8.0) (Sigma) supplemented with a protease inhibitor mixture (Sigma). Cell lysates (20 μg of proteins) were first incubated under denaturing conditions (0.5% SDS and 40 mM DTT) and then treated with 500 units of peptide-*N*-glycosidase F (PNGase F, New England Biolab) during 1 h at 37 °C according to the manufacturer's instructions. Proteins were added to the Laemmli sample buffer in the presence of 0.4 mM 2-mercaptoethanol and electrophoresed on a 8% SDS-polyacrylamide gel alongside the Precision Plus Protein™ dual color standard (Bio-Rad). After electroblotting and blocking with 5% (w/v) skim milk for 30 min, the supported nitrocellulose membranes (Bio-Rad) were incubated with the anti-$Ca_V\alpha2\delta$ (1:750, Alomone Labs, Jerusalem, Israel). Membranes were stripped and incubated with an anti-GAPDH as a loading control (1:10,000, Sigma) unless stated otherwise. Signal was detected with the Bio-Rad ECL chemiluminescent substrate. Blots were visualized with the ChemiDoc Touch documentation system (Bio-Rad). Molecular weights were estimated using Image Lab™ software by linear regression of standard molecular weight markers. The molecular mass of the $Ca_V\alpha2\delta1$ protein in cardiomyocytes was calculated at 123 kDa. The calculated molecular mass of the mCherry-$Ca_V\alpha2\delta1$-HA construct is 153 kDa. GAPDH migrated as a monomer close to 37 kDa in accordance with its calculated mass.

Cycloheximide Chase Assays—Stably transfected $Ca_V\beta3$ cells were transiently transfected simultaneously with pCMV-Ca_V1.2 WT and pmCherry-$Ca_V\alpha2\delta1$-HA WT or NQ mutants. Cells were incubated with 100 μg/ml cycloheximide (Sigma) to block *de novo* protein synthesis 24–36 h after transfection. At the indicated time points (0 h or no cycloheximide, 30 min and 1–4, 6, 10, and 24 h), cell lysates were fractionated on a 8% SDS-PAGE followed by immunoblotting to visualize $Ca_V\alpha2\delta1$ (Alomone Labs, 1:750) and GAPDH (Sigma, 1:10,000). Protein density of $Ca_V\alpha2\delta1$ in total lysates was estimated with Image-Lab 5.2 (Bio-Rad). It was expressed relative to GAPDH and normalized to the relative protein density of $Ca_V\alpha2\delta1$-HA WT measured at time 0. The time course of degradation was measured in 3–5 experiments. Each symbol represents the mean ± S.E. of the normalized protein density.

Isolation of the Plasma Membrane Fraction from Cardiomyocytes and HEKT Cells—Four different protein fractions (total cell lysates, cytosolic, total membrane, and plasma membrane fraction) were prepared according to a protocol published previously (50). Briefly, transfected HEKT cells cultured in 100-mm dishes were homogenized at 4 °C in a Tris-based solution containing a mix of protease inhibitors (Sigma) and 1 mM EDTA, pH 7.4. The cell homogenate was aliquoted into three tubes. After a 2-h incubation period at 4 °C with 1% (v/v) Triton X-100, the first tube was centrifuged at 10,000 × *g* for 10 min to remove cell debris, nuclei, and mitochondria. The supernatant was kept as the total protein fraction (whole-cell lysates). The second tube was centrifuged at 200,000 × *g* and 4 °C for 20 min.

The supernatant is referred to as the cytosolic fraction. The pellet was resuspended in homogenizing buffer containing 1% (v/v) Triton X-100. After 30 min of incubation on ice, a second centrifugation was done at 200,000 × *g*. The resulting supernatant is referred to as the total membrane protein fraction. The third tube was centrifuged at 10,000 × *g* for 10 min. The supernatant obtained was centrifuged at 200,000 × *g* and 4 °C for 20 min. The pellet was resuspended in the homogenizing buffer containing 0.6 M KCl. Subsequent centrifugations were performed at 200,000 × *g* and 4 °C for 20 min to wash out KCl. The final pellet was resuspended in the homogenizing buffer and is considered to be enriched in plasma membrane proteins. Proteins were electrophoresed on an 8% SDS-polyacrylamide gel and blotted with the anti-$Ca_V\alpha2\delta$ (Aviva System Biology 1:1000).

Flow Cytometry Assays—Flow cytometry experiments were conducted as described elsewhere (22). Stable $Ca_V\beta3$ cells were transiently transfected simultaneously with pCMV-$Ca_V1.2$ WT and pmCherry-$Ca_V\alpha2\delta1$-HA WT or mutants. To determine cell surface expression level of the mCherry-$Ca_V\alpha2\delta1$-HA proteins, cells were harvested 24 h after transfection, washed in a 1× PBS buffer, and stained with the FITC-conjugated mouse monoclonal anti-HA epitope tag antibody at 5 μg/ml (Sigma) at 4 °C for 30 min. To determine the total quantity of both intracellular and extracellular expression of the tagged proteins, cells were fixed and permeabilized using BD Cytofix/Cytoperm™ fixation/permeabilization solution kit (BD Biosciences) (22). Roughly 10,000 cells were counted using a FACSAria III® SORP (Special Order Research Product) flow cytometer (BD Biosciences) at the flow cytometry facility hosted by the Department of Microbiologie, Infectiologie, and Immunologie at the Université de Montréal. The level of fluorescence detected with the IgG1-FITC isotype control murine (5 μg/ml) or with the anti-HA FITC-conjugated antibody (5 μg/ml) in HEKT untransfected cells was not significantly different from the fluorescence measured in the complete absence of fluorophore (22). Control conditions were carried out in triplicate with each series of experiments as follows: (*a*) untransfected $Ca_V\beta3$ cells without anti-HA FITC-conjugated antibody; (*b*) untransfected $Ca_V\beta3$ cells with the anti-HA FITC-conjugated antibody to assess the level of background staining; and (*c*) $Ca_V\beta3$ cells transfected with pmCherry-$Ca_V\alpha2\delta1$-HA WT. Expressing the mCherry-$Ca_V\alpha2\delta1$-HA WT constructs in HEKT cells produced a significant 3-log increase in the FITC fluorescence (*x* axis) and mCherry fluorescence (*y* axis) on the two-dimensional plots (22).

Quantification of Steady-state Cell Surface Expression by Flow Cytometry Assays—Flow cytometry data were analyzed using the FlowJo software, version 10 (TreeStar, Ashland, OR) as described (22). Relative expression of $Ca_V\alpha2\delta1$ was calculated based on Δmean fluorescence intensity (ΔMFI) for each fluorophore (mCherry or FITC) as explained elsewhere (22). Briefly, the positive cell gate (P2) and the negative cell gate (P3) were set manually. The fluorescence intensity within the region delineated by the P2 and P3 gates was displayed as cell count *versus* fluorescence intensity. The ΔMFI for FITC was calculated by subtracting the FITC fluorescence density of the FITC-negative cells (P3) from the fluorescence density of the FITC-positive cells (P2). The same method was used to calculate the ΔMFI for mCherry. Under our experimental conditions, the fluorescence intensity follows a normal distribution, hence the mean was equivalent to the median for all intents and purposes. ΔMFI for FITC measured in intact non-permeabilized cells was used as a relative index of the steady-state cell surface density of the HA-tagged $Ca_V\alpha2\delta1$. The ΔMFI values for FITC were measured in permeabilized cells to confirm the accessibility of the HA epitope. It is also a valid estimation of the total protein density because the relative ΔMFI values for FITC estimated in permeabilized cells are comparable with the relative ΔMFI values for mCherry measured under the same conditions. ΔMFI values were normalized to the maximum value measured the same day for mCherry-$Ca_V\alpha2\delta1$-HA WT expressed under the same conditions to account for variations in the absolute fluorescence intensity of the anti-HA FITC-conjugated antibody. The ΔMFI values for FITC and mCherry obtained over the course of several months were pooled and are reported in Table 1, along with the number of triplicate experiments. The normalized ΔMFI values for mCherry measured for each mutant in intact and permeabilized cells were not significantly different from one another ($p > 0.05$) suggesting that the cell permeabilization procedure did not distort significantly the relative fluorescence readout.

Patch Clamp Experiments in HEKT Cells—Whole-cell patch clamp experiments were carried out in isolated cells after transfection in HEKT $Ca_V\beta3$ cells in the presence of the peGFP vector (0.2 μg) as a control for transfection efficiency. Electrodes were filled with a solution containing (in mM) 140 CsCl, 0.6 NaGTP, 3 MgATP, 10 EGTA, 10 HEPES and titrated to pH 7.3 with NaOH. Cells were bathed in a modified Earle's saline solution (in mM) containing 135 NaCl, 20 TEACl, 2 $CaCl_2$, 1 $MgCl_2$, 10 HEPES and titrated to pH 7.3 with KOH. On-line data acquisition was achieved with the Axopatch 200-B amplifier (Molecular Devices, Sunnyvale, CA) connected with the PClamp software Clampex 10.5 through the Digidata 1440A acquisition system (Molecular Devices) (22). A series of 450-ms voltage pulses were applied from a holding potential of −100 mV at a frequency of 0.2 Hz, from −60 to +70 mV at 5-mV intervals. Series resistance was compensated to ~85% after on line capacitive transient cancellation. Unless stated otherwise, whole-cell currents were sampled at 5 kHz and filtered at 1 kHz. PClamp software Clampfit10.5 was used for data analysis. Mid-potential of activation values ($E_{0.5,act}$) were estimated from the peak *I-V* curves obtained for each channel composition and were reported as the mean of individual measurements ± S.E (Table 2) (22, 53). The free energy of activation was calculated using the mid-activation potential as shown in Equation 1,

$$\Delta G_{act} = z \cdot F \cdot E_{0.5\,act} \quad \text{(Eq. 1)}$$

where *z* is the effective charge displacement during activation, and *F* is the Faraday constant (54). The r100 ratio is defined as the ratio of peak whole-cell currents remaining after a depolarizing pulse of 100 ms (I_{100ms}/I_{Peak}) and was used as an indicator of the inactivation kinetics. The pmCherry-$Ca_V\alpha2\delta1$-HA construct was previously shown to carry the functional modulation of $Ca_V1.2$ currents (22). Each novel pmCherry-$Ca_V\alpha2\delta1$-HA

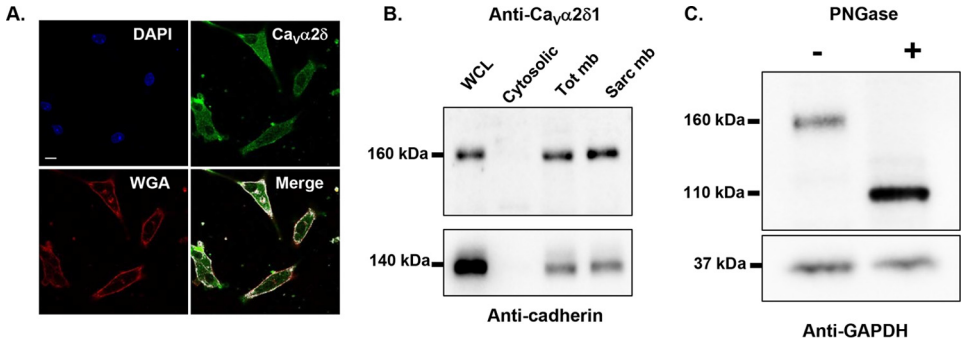

FIGURE 1. *A,* endogenous $Ca_V\alpha2\delta1$ proteins in mouse cardiomyocytes are glycoproteins. Endogenous $Ca_V\alpha2\delta1$ in 24-h cultured mouse cardiomyocytes co-localized with wheat germ agglutinin 647 (WGA 647), a plasma membrane marker that displays a high affinity for glycoproteins. $Ca_V\alpha2\delta1$ proteins were stained with the anti-$Ca_V\alpha2\delta1$ as the primary antibody and Alexa 488-coupled secondary antibody. *Scale bar* corresponds to 10 μm. The *red* channel was arbitrarily assigned to WGA, and the *green* channel was assigned to $Ca_V\alpha2\delta1$. Nuclei are stained with DAPI (*blue*). Co-localization pixel maps of $Ca_V\alpha2\delta1$ and WGA are shown in *white* and were produced using the co-localization finder plugin in FIJI. *B,* endogenous $Ca_V\alpha2\delta1$ proteins in the sarcolemmal membrane fraction of mouse cardiomyocytes migrate at 160 kDa. Four different protein fractions (total (*WCL*), cytosolic (*Cyto*), total membrane (*Tot mb*), and sarcolemmal membrane (*Sarc mb*)) were isolated from ventricles of adult CD-1 mice (50). Proteins were electrophoresed on an 8% SDS-polyacrylamide denaturating gel, transferred to a nitrocellulose membrane, and probed with an anti-$Ca_V\alpha2\delta1$ (Aviva System Biology). The membrane was probed, after stripping, with anti-pan-cadherin (Invitrogen 1:5000) as a quality control for the fractionation process. It is worth noting that the 160-kDa protein is the dominant species in whole-cell lysates. Each lane was loaded with 10 μg of proteins. *C,* PNGase F-mediated deglycosylation of the *N*-linked sugars in endogenous $Ca_V\alpha2\delta1$ proteins from mouse cardiomyocytes. Total whole-cell proteins isolated from ventricles of adult CD-1 mice were denatured 20 min at 60 °C before incubation in the absence (−) or presence (+) of PNGase F during 1 h at 37 °C. Each lane was loaded with 20 μg of proteins. Proteins were electrophoresed on an 8% SDS-polyacrylamide denaturing gel, transferred to a nitrocellulose membrane, and probed with an anti-$Ca_V\alpha2\delta1$ (Alomone Labs) (*top panel*) and anti-GAPDH (*bottom panel*) as a loading control.

mutant was tested alongside the control WT construct (pCMV-$Ca_V1.2$ WT + pmCherry-$Ca_V\alpha2\delta1$-HA WT with $Ca_V\beta3$ cells) to assess for internal consistency thus explaining the large sample size for the mCherry-$Ca_V\alpha2\delta1$-HA WT construct. Experiments performed under the same conditions yielded peak current densities that could vary by as much as ±35% between each series of experiments. This variation appeared to be essentially linked to minor changes in the cell density at the time of transfection. Data from all experiments performed under the same conditions over a period of 16 months were pooled, and biophysical properties are reported in Table 2. Experiments were performed at room temperature (18–20 °C).

Statistics—Results were expressed as mean ± S.E. Tests of significance were carried out using the unpaired analysis of variance with the Tukey test embedded in the Origin 7.0 analysis software (OriginLab Corp., Northampton, MA). Data were considered statistically significant at $p < 0.05$.

Results

Cardiac $Ca_V\alpha2\delta1$ Proteins Are Glycosylated—$Ca_V\alpha2\delta1$ is largely believed to be the most heavily glycosylated protein within the cardiac L-type channel complex (32). Triple-color immunostaining of cultured mouse cardiomyocytes with wheat germ agglutinin (WGA), a plasma membrane marker that binds glycoproteins with high affinity, DAPI, a marker for the nucleus, and an anti-$Ca_V\alpha2\delta1$ demonstrated that the glycoprotein $Ca_V\alpha2\delta1$ co-localized with WGA (Fig. 1*A*). The expression of the endogenous $Ca_V\alpha2\delta1$ in the sarcolemmal membrane-enriched fraction in mouse cardiomyocytes was confirmed by membrane fractionation followed by SDS-PAGE. As seen, the major protein species migrated at an apparent molecular mass of 160 kDa in all fractions (Fig. 1*B*), which is similar to the mobility of the $Ca_V\alpha2\delta1$ protein expressed in brain (29). Given that the calculated molecular mass of the rodent $Ca_V\alpha2\delta1$ is 124 kDa, this suggests the native protein undergoes significant co- or post-translational modifications. To note, partially glycosylated species were not detected under our experimental conditions. Enzymatic deglycosylation carried out with PNGase F, an amidase that removes all saccharide moieties and reduced the electrophoretic mobility of the endogenous protein from 160 to 110 kDa (Fig. 1*C*). The 50-kDa decrease in the mobility of endogenous $Ca_V\alpha2\delta1$ is compatible with the addition of *N*-glycans onto 10–14 *N*-glycosylation sites (26, 27, 31).

Molecular Identification of N-Glycosylation Sites in $Ca_V\alpha2\delta1$—By definition, *N*-linked glycans are attached to the nitrogen atom of an asparagine side chain within the Asn-Xaa-(Ser/Thr) consensus sequence, where Xaa is not a proline residue. It is estimated that at least two-thirds of those sites are likely to be *N*-glycosylated (55). Using this strict definition, we identified 16 putative glycosylation sites in the extracellular portion of the $Ca_V\alpha2\delta1$ protein as follows: Asn-92, Asn-136, Asn-184, Asn-324, Asn-348, Asn-468, Asn-475, Asn-585, Asn-594, Asn-663, Asn-769, Asn-812, Asn-876, Asn-883, Asn-973, and Asn-986 in the rat isoform (Fig. 2*A* and data not shown). Seven sites are conserved in the primary sequence of the human, rat, and mouse $Ca_V\alpha2\delta1$ as follows: Asn-92, Asn-184, Asn-348, Asn-468, Asn-594, Asn-663, and Asn-812. The Asn-348 and Asn-468 sites are also conserved in $Ca_V\alpha2\delta2$. Many Asn-Xaa-Ser sites are glycosylated inefficiently *in vitro* (56), whereas Asn-Xaa-Thr sites are usually efficiently glycosylated. Even though the presence of the Asn-Xaa-(Ser/Thr) site is necessary for the receipt of an *N*-glycan, transfer of the *N*-glycan to this site does not always occur, due to conformational or other constraints during glycoprotein folding (55). Enzymatic digestion with PNGase F carried out with whole-cell lysates from recombinant $Ca_V\alpha2\delta1$ expressed in HEKT cells also demonstrated a reduction of 50 kDa in the electrophoretic mobility of $Ca_V\alpha2\delta1$ (Fig. 2*B*), similar to the one observed above for the endogenous $Ca_V\alpha2\delta1$ protein. The mobility shift assay also suggests that the $Ca_V\delta$ protein may not be proteolytically

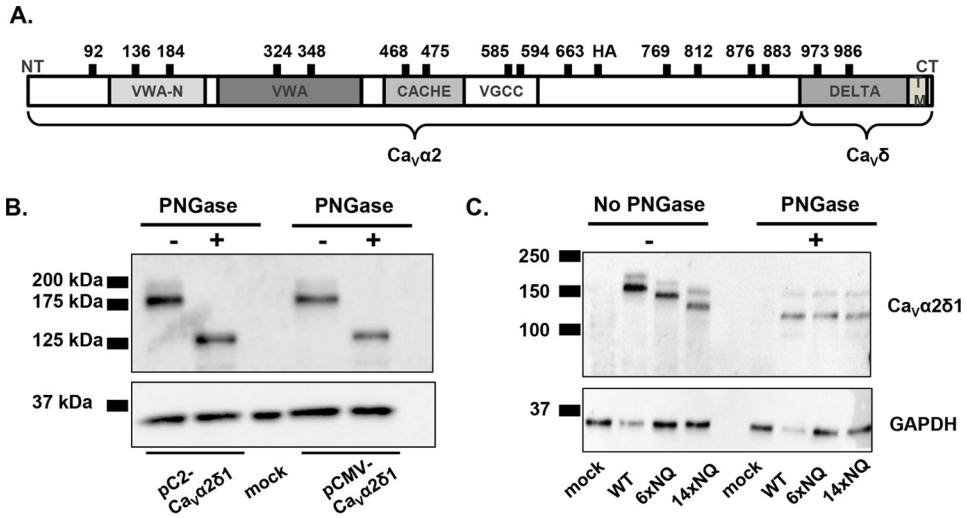

FIGURE 2. **PNGase F-mediated deglycosylation of the *N*-linked sugars from Ca$_V$α2δ1 expressed in HEKT.** *A,* relative positions of the predicted *N*-glycosylation sites are shown on the structural domains of the rat Ca$_V$α2δ1. Structural domains were identified using protein BLAST (blast.ncbi.nlm.nih.gov) with the UniProtKB/Swiss-Prot database. The four structural domains are shown by *boxes*: *VWAN* (NCBI pfam08399), *VWA* (NCBI smart00327), *CACHE* (NCBI pfam02743), and *VGCC* (NCBI pfam08473). *B,* cells were transiently transfected with pCMV-Ca$_V$α2δ1 or pC2-Ca$_V$α2δ1. Total cell lysates were extracted 24 h after transfection using the protocol described earlier. Total cell lysates were denatured 10 min at 95 °C before incubation in the absence (−) or presence (+) of PNGase during 1 h at 37 °C. Proteins were electrophoresed on a 8% SDS-polyacrylamide denaturating gel, transferred to a nitrocellulose membrane, and probed with an anti-Ca$_V$α2δ1 (Alomone Labs) and anti-GAPDH as a loading control. Each lane was loaded with 10 μg of proteins. As seen, the electrophoretic mobility of the Ca$_V$α2δ1 protein decreased by 50 kDa following enzymatic digestion. *C,* mutations of multiple glycosylation sites decreased protein mobility. HEKT cells were transiently transfected with pmCherry-Ca$_V$α2δ1-HA WT, 6xNQ, or 14xNQ. Exactly 24 h after transfection, cells were lysed, and protein lysates were either treated with the vehicle buffer or with PNGase F during 1 h at 37 °C. Proteins were fractionated by SDS-PAGE (8%). Western blot analysis was carried out with the Ca$_V$α2δ1 antibody (Alomone Labs) as the primary antibody, and signal was detected using the Bio-Rad ECL substrate. The *2nd lanes* (± *PNGase*) were loaded with 5 μg of proteins, and the *1st, 3rd,* and *4th lanes* were loaded with 10 μg. *1st lane,* mock-transfected HEKT cells; *2nd lane,* pmCherry-Ca$_V$α2δ1-HA WT; *3rd lane,* pmCherry-Ca$_V$α2δ1-HA 6xNQ; *4th lane,* pmCherry-Ca$_V$α2δ1-HA 14xNQ. The calculated molecular masses for the high density band are before treatment with PNGase as follows: *2nd lane,* 171 kDa; *3rd lane,* 155 kDa; *4th lane,* 133 kDa; after digestion with PNGase: *2nd lane,* 123 kDa; *3rd lane,* 123 kDa; and *4th lane,* 123 kDa. The 10-kDa difference in the molecular masses between the 14xNQ before and after treatment with PNGase could suggest that *N*-glycosylation was not completely eliminated in the 14xNQ mutant or else that the enzymatic treatment itself altered the migration of the protein in the gel.

cleaved under our experimental conditions (57, 58). The molecular determinants responsible for N-type glycosylation were investigated using a mutational analysis. Multiple Asn to Gln mutants were produced in the pmCherry-Ca$_V$α2δ1-HA construct that was previously shown to be expressed at the plasma membrane and fully functional (22). The glycosylation status of multiple constructs 6xNQ (N92Q/N184Q/N348Q/N594Q/N812Q/N876Q) that includes the six Asn sites that were predicted to be the most likely to be glycosylated and the 14xNQ construct (N92Q/N136Q/N184Q/N348Q/N468Q/N585Q/N594Q/N663Q/N769Q/N812Q/N876Q/N883Q/N986Q/N1066Q) that includes the 14 Asn sites with a likelihood above 0.5 (59) were first investigated. Western blots produced with whole-cell lysates showed that pmCherry-Ca$_V$α2δ1-HA WT migrated as a doublet with a faint band at ≈200 kDa and a stronger band ≈175 kDa (Fig. 2*C*). The 6xNQ and the 14xNQ proteins produced a band pattern of significantly weaker intensity with protein mobility reduced by ≈25 and ≈45 kDa, respectively (Fig. 2*C*), suggesting that acquisition of *N*-glycans was not completely impaired in the 6xNQ and the 14xNQ mutants. Indeed, enzymatic digestion with PNGase F further reduced the electrophoretic mobility and produced similar migration profiles for the mCherry-Ca$_V$α2δ1-HA WT, 6xNQ, and the 14xNQ proteins. Altogether, this observation supports the view that some of the Asn residues mutated in the 6xNQ construct (Asn-92, Asn-184, Asn-348, Asn-594, Asn-812, and/or Asn-876), some of the additional residues substituted in the 14xNQ construct (Asn-136, Asn-468, Asn-585, Asn-663, Asn-769, Asn-883, Asn-986, and/or Asn-1066), and possibly the two remaining residues (Asn-475 and Asn-973) are acquiring *N*-glycans either co-translationally or post-translationally.

Disrupting Six Asn Sites Impaired Steady-state Surface Density of Ca$_V$α2δ1—To evaluate whether the partially glycosylated forms reach the plasma membrane, we quantified the cell surface fluorescence of the mCherry-Ca$_V$α2δ1-HA WT and NQ constructs in two-color flow cytometry assays. In this construct, the mCherry fluorescence is constitutive. The fluorescence of the FITC-conjugated HA antibody was shown to be proportional to the fraction of proteins present at the cell surface because the HA epitope is located in the extracellular portion of Ca$_V$α2δ1 (22). The fluorescence intensity ΔMFI for FITC measured in intact cells, observed as a rightward shift in the fluorescence intensity on the *x* axis of the two-dimensional plots, provides a reliable index of the steady-state cell surface density of Ca$_V$α2δ1. The mCherry epitope expressed at the C terminus of the construct, observed as an increase in the fluorescence intensity seen on the *y* axis of the two-dimensional plots, served as a marker for total protein expression. The two-color assay thus provided a quick and reliable readout of protein expression. Control experiments carried out with the mCherry-Ca$_V$α2δ1 WT control construct that was not HA-tagged confirmed the specificity of the FITC antibody in these series of experiments (Fig. 3*A*). The fluorescence histograms for the corresponding experiment were reported to the right of the contour plots, whereas the averaged mean fluorescence intensity

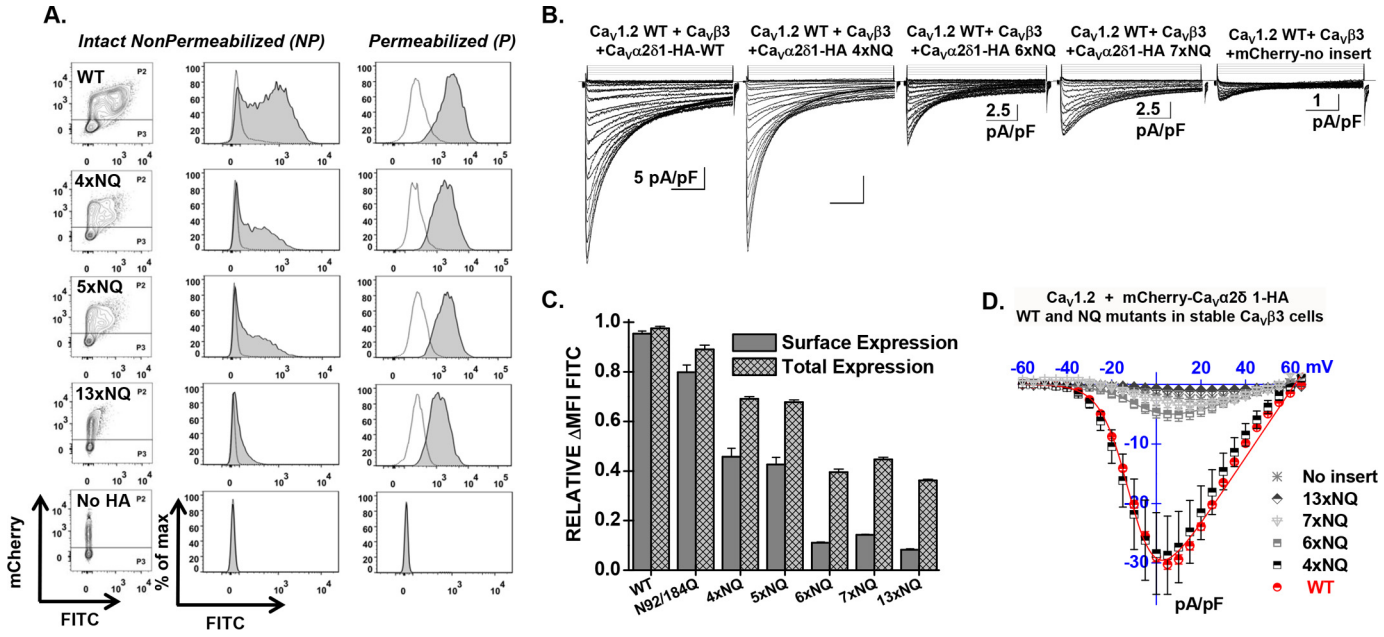

FIGURE 3. **Simultaneous mutations of six *N*-glycosylation sites disrupt cell surface expression of $Ca_V\alpha2\delta1$ and prevent the stimulation of $Ca_V1.2$ currents.** Stable $Ca_V\beta3$ cells were transiently transfected simultaneously with pCMV-$Ca_V1.2$ WT and pmCherry-$Ca_V\alpha2\delta1$-HA WT or mutants. *A,* representative two-dimensional plots of mCherry *versus* FITC fluorescence are shown for each *N*-glycosylation mutants (NQ) after the disruption of four sites (4xNQ), five sites (5xNQ), and 13 sites (13xNQ). The *No HA* construct is mCherry-$Ca_V\alpha2\delta1$ WT. The distribution of the fluorescence intensity measured for cells within the P2 gate (fluorescence-positive cells) are shown in *gray,* and the distribution of fluorescence intensity for cells present in the P3 gate (fluorescence-negative cells) is displayed as an overlay in a transparent *gray plot*. In all cases, the ΔMFI fluorescence measured for FITC in permeabilized cells was qualitatively similar to the constitutive fluorescence measured for mCherry validating the accessibility of the HA epitope and confirming the values obtained for total protein expression. Numerical values are shown in Table 1 and data not shown. *B,* representative whole-cell Ca^{2+} current traces obtained after recombinant expression of $Ca_V1.2$ in stable $Ca_V\beta3$ cells with mCherry-$Ca_V\alpha2\delta1$-HA WT or mCherry-$Ca_V\alpha2\delta1$-HA glycosylation NQ mutants. The same mCherry-$Ca_V\alpha2\delta1$-HA constructs were used for the flow cytometry assays and the patch clamp experiments. Currents were recorded in the presence of 2 mM Ca^{2+} from a holding potential of −100 mV. Time scale is 100 ms throughout. Unless specified otherwise, the current density scale is 5 pA/pF. Co-expression with $Ca_V\alpha2\delta1$ shifted the voltage dependence of activation of $Ca_V1.2$ WT/$Ca_V\beta3$ from $E_{0.5,\,act} = 8 \pm 2$ mV ($n = 35$) (no $Ca_V\alpha2\delta1$) to $E_{0.5,\,act} = -9.4 \pm 0.2$ mV ($n = 231$) (for $Ca_V1.2$ WT/$Ca_V\beta3$ with mCherry-$Ca_V\alpha2\delta1$-HA WT), a significant −15-mV shift in the activation potential. The free energy of activation (ΔG_{act}) measured in the presence of mCherry-$Ca_V\alpha2\delta1$-HA WT was well described by a Gaussian distribution centered at -0.86 ± 0.2 kcal mol^{-1} ($n = 231$). *C, bar graph* shows the normalized ΔMFI measured in the presence of FITC in intact (surface expression) or permeabilized cells (total expression) in flow cytometry experiments. *D,* averaged current-voltage relationships, recorded in the presence of 2 mM Ca^{2+}, are shown for mCherry-$Ca_V\alpha2\delta1$-HA WT, and the multiple mCherry-$Ca_V\alpha2\delta1$-HA mutants 4xNQ (N92Q/N348Q/N594Q/N876Q), 6xNQ (N92Q/N184Q/N348Q/N594Q/N812Q/N876Q), 7xNQ (N92Q/N184Q/N348Q/N594Q/N812Q/N876Q/N986Q), 13xNQ (N92Q/N136Q/N184Q/N348Q/N468Q/N585Q/N594Q/N769Q/N812Q/N876Q/N883Q/N986Q/N1066Q). Currents traces obtained with the mCherry vector are also shown. See Tables 1 and 2 for analysis of the statistical significance.

values (ΔMFI) obtained from ≥3 distinct experiments are shown in Fig. 3*C*. As seen, the fluorescence intensity ΔMFI for FITC in intact nonpermeabilized cells was strong for the WT and the 4xNQ construct but sharply decreased from the 5xNQ to the 13xNQ constructs (data not shown). These constructs produced proteins that were almost absent from the cell surface. Nonetheless, a slightly different version of the 6xNQ mutant (N92Q/N184Q/N468Q/N594Q/N876Q/N986Q) was present at the cell surface at a density similar to the 4xNQ mutant (data not shown). Assays were also conducted after cell permeabilization, and the fluorescence histograms shown alongside confirmed the accessibility of the HA epitope. Altogether, these results suggest the following: 1) mutations of consensus *N*-glycosylation sites are associated with decreased steady-state cell surface density of $Ca_V\alpha2\delta1$; 2) mutations of consensus *N*-glycosylation sites impaired total protein density; and 3) *N*-glycosylation sites may not all be functionally equivalent.

Disrupting Asn Sites Impairs Channel Function—Mutating the consensus *N*-linked glycosylation reduced the steady-state cell surface density of the $Ca_V\alpha2\delta1$ protein. Its impact on the L-type $Ca_V1.2$ channel function was explored after recombinant expression of $Ca_V1.2$ with mCherry-$Ca_V\alpha2\delta1$-HA multiple NQ mutants in stable $Ca_V\beta3$ cells. As reported before (22), co-expression of pmCherry-$Ca_V\alpha2\delta1$-HA WT with $Ca_V1.2$ WT in stable $Ca_V\beta3$ cells stimulated whole-cell peak current densities from -3 ± 1 pA/pF ($n = 35$) (no insert in the pmCherry vector) to -30 ± 1 pA/pF ($n = 231$) in the presence of $Ca_V\alpha2\delta1$ WT (Fig. 3, *B* and *D*). The increase in peak current densities was associated with an ≈ −15-mV leftward shift in the activation potential of $Ca_V1.2$ from $E_{0.5,\,act} = 8 \pm 2$ mV ($n = 35$) (no $Ca_V\alpha2\delta1$) to $E_{0.5,\,act} = -9.6 \pm 0.1$ mV ($n = 231$) (with mCherry-$Ca_V\alpha2\delta1$-HA). As seen, co-expression with mCherry-$Ca_V\alpha2\delta1$-HA mutants containing 4 (4xNQ), 6 (6xNQ), and 13 (13xNQ) mutations yielded voltage-activated Ca^{2+} currents. Mutating four sites did not appreciably alter whole-cell peak current density, but mutations of two additional consensus sites in the 6xNQ mutant (N92Q/N184Q/N348Q/N594Q/N812Q/N876Q) was sufficient to significantly decrease by 6-fold the peak current density of $Ca_V1.2$ currents. Furthermore, peak current densities measured with the 13xNQ mutant were not statistically different from Ca^{2+} currents obtained in the absence of $Ca_V\alpha2\delta1$ (data not shown). These results suggest that residues Asn-184 and Asn-812 could be among the most critical residues in carrying channel modulation.

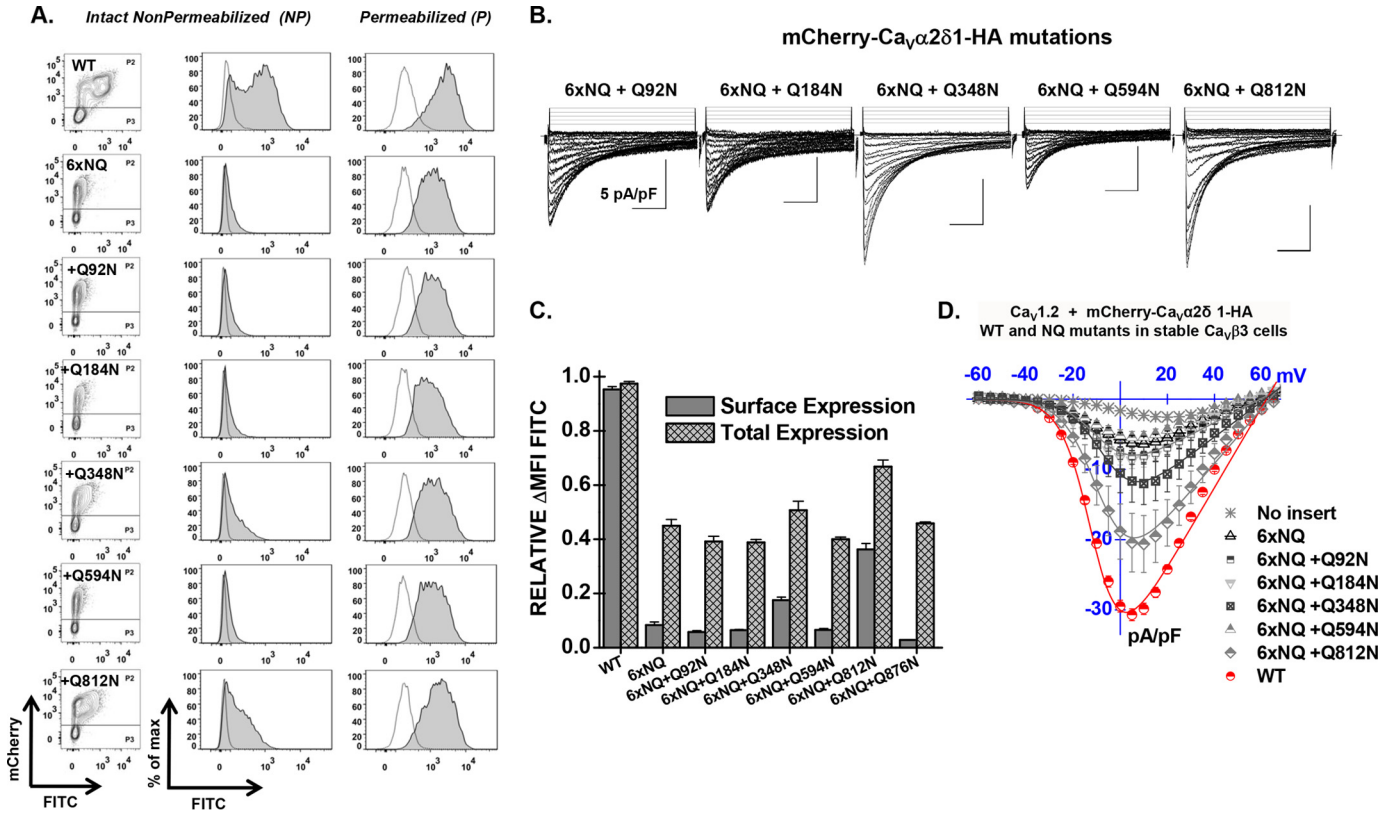

FIGURE 4. **Reverse mutation Q812N cancels the impact of the 6xNQ mutant on $Ca_V\alpha2\delta1$.** *A,* representative two-dimensional plots of mCherry *versus* FITC fluorescence are shown for each *N*-glycosylation mutant (NQ). The 6xNQ construct (N92Q/N184Q/N348Q/N594Q/N812Q/N876Q) was used as a template from which single point reverse mutations were introduced as indicated. As seen, only the reverse mutations Q348N and Q812N effectively expressed at the cell surface. *B,* representative whole-cell Ca^{2+} current traces obtained after recombinant expression of $Ca_V1.2$ in stable $Ca_V\beta3$ cells with mCherry-$Ca_V\alpha2\delta1$-HA WT or mCherry-$Ca_V\alpha2\delta1$-HA *N*-glycosylation mutants (NQ). *C, bar graph* shows the normalized ΔMFI measured in the presence of FITC in intact (surface expression) or permeabilized cells (total expression) in flow cytometry experiments. *D,* averaged current-voltage relationships, recorded in the presence of 2 mM Ca^{2+}, are shown for the reverse mutations mCherry-$Ca_V\alpha2\delta1$-HA 6xNQ + Q92N (N184Q/N348Q/N594Q/N812Q/N876Q); 6xNQ + Q184N (N92Q/N348Q/N594Q/N812Q/N876Q); 6xNQ + Q348N (N92Q/N184Q/N594Q/N812Q/N876Q); 6xNQ+ 594N (N92Q/N184Q/N348Q/N812Q/N876Q); and 6xNQ + Q812N (N92Q/N184Q/N348Q/N594Q/N876Q). As a control for relative expression, functional modulation by mCherry-$Ca_V\alpha2\delta1$-HA WT was measured under the same conditions (data not shown). See Tables 1 and 2 for statistical significance.

Only a Few Asn Residues Contribute to $Ca_V\alpha2\delta1$ Function—Cell surface density, protein stability, and channel function were significantly impaired in the 6xNQ construct. To identify the individual contribution of each residue to the functional response, reverse Gln to Asn mutations were introduced in the 6xNQ construct. As seen, reinstating the Asn-812 site, with the "6xNQ + Q812N" mutant, nearly restored the steady-state cell surface density of $Ca_V\alpha2\delta1$ and L-type channel function (Fig. 4, *A* and *B*). Reintroducing Asn-348 with the "6xNQ + Q348N" mutant was also seen to significantly improve cell surface density and channel function. These data suggest that N348Q could account for the large decrease in the cell surface density of the 4xNQ mutant. In both cases, the increase in the relative cell surface density of $Ca_V\alpha2\delta1$ (Fig. 4*C*) was correlated with an augmentation of the peak current density as compared with the 6xNQ mutant (Fig. 4*D*). In addition, the mean ΔMFI for FITC in permeabilized cells (an index of total cell density) increased in these two reverse mutants suggesting that protein stability and/or synthesis was also improved as compared with the 6xNQ mutant (Fig. 4*C*). The individual impact of each Asn site was finally investigated in single point mutations. Sixteen single Asn to Gln mutations were tested (N92Q; N136Q; N184Q; N324Q; N348Q; N468Q; N475Q; N585Q; N594Q; N663Q; N769Q; N812Q; N812A; N876Q; N883Q; N973Q; and N986Q) (Fig. 5 and Table 1). Most single mutations only caused small changes in the relative fluorescence intensity at the cell surface without significant change in channel gating, suggesting that these single mutants reached the cell surface in their native conformation. One can suppose that small changes in the surface fluorescence could result from minor alterations in the protein trafficking or protein conformation. Nine mutations (N136Q; N324Q; N475Q; N585Q; N594Q; N769Q; N876Q; N883Q; and N986Q) produced fluorescent patterns for FITC and mCherry not significantly different ($p > 0.05$) than the wild-type construct suggesting that neither surface density nor protein stability was affected by these single mutations. Three single mutations mCherry-$Ca_V\alpha2\delta1$-HA N92Q, mCherry-$Ca_V\alpha2\delta1$-HA N184Q, and mCherry-$Ca_V\alpha2\delta1$-HA N973Q produced proteins that yielded slightly smaller fluorescent signals (by ≈15–20%) than the control mCherry-$Ca_V\alpha2\delta1$-HA WT construct ($p < 0.05$). However, all these above-mentioned single NQ mutants stimulated peak currents to the same extent as the wild-type construct ($p > 0.05$) (Table 2).

Four single point mutations (N348Q; N468Q; N663Q; and N812Q) significant decreased the fluorescence at the cell surface ($p < 0.001$). The strongest impact produced by a single

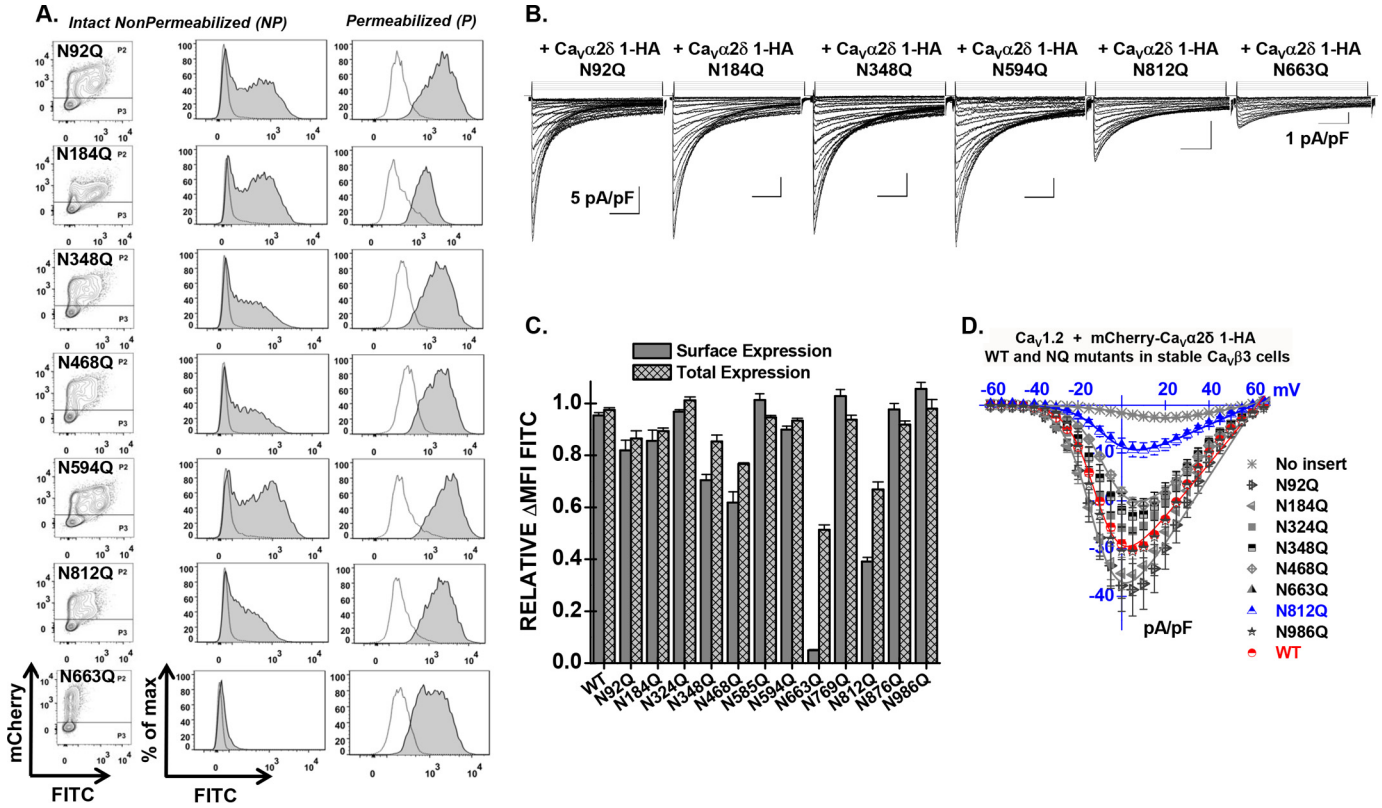

FIGURE 5. **Single mutations N663Q and N812Q decrease cell surface expression of $Ca_V\alpha2\delta1$ and modulation of $Ca_V1.2$ whole-cell currents.** *A,* representative two-dimensional plots of mCherry *versus* FITC fluorescence are shown for each mutation as stated. *B,* representative whole-cell Ca^{2+} current traces recorded after recombinant expression of $Ca_V1.2$ in stable $Ca_V\beta3$ cells with mCherry-$Ca_V\alpha2\delta1$-HA WT or some *N*-glycosylation single mutants. Unless specified otherwise, the current density scale is 5 pA/pF. Functional modulation by mCherry-$Ca_V\alpha2\delta1$-HA WT was measured under the same experimental conditions (data not shown). *C, bar graph* shows the normalized ΔMFI measured in the presence of FITC in intact (surface expression) or permeabilized cells (total expression). *D,* current-voltage relationships, recorded in the presence of 2 mM Ca^{2+}, are shown for the single mutations mCherry-$Ca_V\alpha2\delta1$-HA N92Q, mCherry-$Ca_V\alpha2\delta1$-HA N184Q, mCherry-$Ca_V\alpha2\delta1$-HA N324Q, mCherry-$Ca_V\alpha2\delta1$-HA N348Q, mCherry-$Ca_V\alpha2\delta1$-HA N468Q, mCherry-$Ca_V\alpha2\delta1$-HA N663Q, mCherry-$Ca_V\alpha2\delta1$-HA N812Q, and mCherry-$Ca_V\alpha2\delta1$-HA N986Q. Statistical significance is reported Tables 1 and 2.

mutation was obtained with N663Q that eradicated cell surface fluorescence and channel function (Fig. 5 and Tables 1 and 2). N812Q and N812A also produced proteins that significantly decreased cell surface fluorescence. Data from the flow cytometry assays were corroborated with confocal images captured with live cells stained with the FITC-conjugated anti-HA tag antibody. Cell surface fluorescence intensity decreased sharply for the 6xNQ mutant and was noticeably weaker for the single N812Q mutant than for the wild-type construct (Fig. 6). In agreement with the fluorescence data, N812Q generated currents that were twice larger than the 6xNQ mutant but ≈3 times smaller than currents produced with the wild-type construct ($p < 0.01$) (Table 2).

The potentially additive effect of these residues (save for N663Q that was already non-functional on its own) was investigated in double mutants. Pairing Asn sites in different combinations, to form double mutants N348Q/N468Q, N348Q/N812Q, and N468Q/N812Q, produced proteins that significantly reduced the steady-state cell surface density of $Ca_V\alpha2\delta1$ and modulation of $Ca_V1.2$ currents (Fig. 7, Tables 1 and 2; and data not shown). Pairing N92Q with either N348Q, N468Q, or N812Q as one of the partners yielded voltage-activated currents that were roughly 50% lower than produced with the wild-type construct. In contrast, other mCherry-$Ca_V\alpha2\delta1$-HA double NQ mutants (N92/N184Q, N92Q/N594Q, N136Q/N184Q, N136Q/N769Q, and N594Q/N876Q) produced whole-cell currents similar to the mCherry-$Ca_V\alpha2\delta1$-HA WT construct ($p > 0.05$). The series of wild-type-like double mutants include N136Q/N184Q previously shown to prevent the subunit-mediated regulation of $Ca_V2.2$ currents (60). These results suggest that Asn-348, Asn-468, Asn-663, and Asn-812 in $Ca_V\alpha2\delta1$ play unique roles in the modulation of $Ca_V1.2$.

Mutations of these sites produced $Ca_V\alpha2\delta1$ proteins with impaired *N*-glycosylation. Mobility shift assays were carried out before and after digestion with PNGase F in three separate series of experiments as follows: with double mutants N136Q/N184Q, N348Q/N468Q, N348Q/N812Q, and N468Q/N812Q (Fig. 8*A*), multiple mutants that were not detected at the membrane N348Q/N468Q/N812Q and N92Q/N184Q/N348Q/N468Q/N594Q/N812Q (Fig. 8*B*), and single N663Q (Fig. 8*C*). Under control conditions, there was a small but significant decrease in the protein mobility (<10 kDa) for the double mutants when compared with the WT construct and a smaller one with single mutants, although this was not always clearly evident. Digestion with PNGase F decreased the electrophoretic mobility of N663Q, as well as the double, triple, and sextuple mutants, respectively by 48, 45, 40, and 30 kDa, respec-

TABLE 1

Relative fluorescence intensity ΔMFI for Cherry-$Ca_v\alpha2\delta1$-HA WT and mutants

$Ca_v1.2$ WT was co-expressed in stable $Ca_v\beta3$ HEKT cells with pmCherry-$Ca_v\alpha2\delta1$-HA WT or mutant using a 1:1 DNA ratio. Flow cytometry experiments were conducted to determine cell surface expression levels of tagged proteins, and fluorescence intensity was measured with the FlowJo software as described under "Experimental Procedures." Relative expression of $Ca_v\alpha2\delta1$ was calculated based on ΔMFI estimated for each fluorophore (mCherry or FITC). ΔMFI for FITC measured in intact non-permeabilized cells was used as an index of the cell surface density of the HA-tagged $Ca_v\alpha2\delta1$, and ΔMFI values for FITC measured in permeabilized cells reflect the total protein expression (cell surface and intracellular protein density). The ΔMFI values for the mCherry-$Ca_v\alpha2\delta1$-HA mutants were pooled and normalized to the maximum value obtained for pmCherry-$Ca_v\alpha2\delta1$-HA WT that was expressed under the same conditions and measured the same day. The total number of experiments is provided in parentheses. The ΔMFI values for FITC measured in permeabilized cells were mostly similar to the ΔMFI for mCherry measured in intact and permeabilized cells. Furthermore, the ΔMFI values for mCherry measured in intact and permeabilized cells were found to be within experimental error suggesting that cell permeabilization did not significantly alter the protein structure. Statistical analysis was carried out against the ΔMFI for FITC measured with pmCherry-$Ca_v\alpha2\delta1$-HA WT (* $p < 0.05$; ** $p < 0.01$).

mCherry- $Ca_V\alpha2\delta1$-HA mutant with $Ca_V1.2$ WT in $Ca_V\beta3$ stable HEKT cells	ΔMFI FITC		ΔMFI mCherry	
	Intact cells *(Relative surface density)*	**Perm cells** *(Relative total density)*	**Intact cells** *(Relative total density)*	**Perm cells** *(Relative total density)*
+ mCherry-$Ca_V\alpha2\delta1$-HA WT	0.96 ± 0.02 (66)	0.97 ± 0.01 (66)	0.97 ± 0.01 (66)	0.97 ± 0.01 (66)
N92Q	0.82 ± 0.04 (12)*	0.87 ± 0.02 (12)*	0.86 ± 0.05 (12)*	0.88 ± 0.04 (12)*
N136Q	0.98 ± 0.03 (3)	0.98 ± 0.03 (3)	1.02 ± 0.04 (3)	1.1 ± 0.1 (3)
N184Q	0.86 ± 0.04 (6)*	0.89 ± 0.01 (6)*	0.93 ± 0.02 (6)	0.86 ± 0.03 (6)*
N324Q	0.97 ± 0.01 (6)	1.02 ± 0.01 (6)	0.99 ± 0.01 (6)	1.01 ± 0.02 (6)
N348Q	0.68 ± 0.02 (12)**	0.86 ± 0.02 (12)*	0.84 ± 0.01 (12)*	0.85 ± 0.01 (12)*
N468Q	0.62 ± 0.04 (9)**	0.84 ± 0.03 (9)*	0.79 ± 0.01 (9)**	0.79 ± 0.01 (9)**
N475Q	1.01 ± 0.01 (3)	1.04 ± 0.02 (3)	1.04 ± 0.02 (3)	0.97 ± 0.02 (3)
N585Q	1.01 ± 0.02 (3)	0.94 ± 0.01 (3)	0.94 ± 0.02 (3)	0.89 ± 0.01 (3)
N594Q	0.93 ± 0.01 (3)	0.93 ± 0.01 (3)	0.94 ± 0.01 (3)	0.94 ± 0.02 (3)
N663Q	0.05 ± 0.01 (3)**	0.51 ± 0.02 (3)**	0.76 ± 0.02 (3)*	0.73 ± 0.03 (3)*
N769Q	1.02 ± 0.02 (3)	0.94 ± 0.02 (3)	0.91 ± 0.01 (3)	0.88 ± 0.01 (3)
N812Q	0.39 ± 0.02 (12)**	0.73 ± 0.04 (12)*	0.85 ± 0.04 (12)*	0.81 ± 0.03 (12)*
N812A	0.40 ± 0.01 (3)**	0.70 ± 0.01 (3)*	0.77 ± 0.01 (3)*	0.77 ± 0.01 (3)*
N876Q	0.98 ± 0.02 (3)	0.92 ± 0.01 (3)	0.98 ± 0.02 (3)	0.96 ± 0.02 (3)
N883Q	0.96 ± 0.02 (3)	0.93 ± 0.01 (3)	0.97 ± 0.02 (3)	0.95 ± 0.02 (3)
N973Q	0.76 ± 0.03 (3)*	0.96 ± 0.03 (3)	0.89 ± 0.04 (3)*	0.81 ± 0.03 (3)*
N986Q	1.01 ± 0.05 (6)	0.98 ± 0.04 (6)	1.03 ± 0.05 (6)	0.94 ± 0.05 (6)
N92Q/N184Q	0.80 ± 0.03 (6)*	0.95 ± 0.01 (6)	0.88 ± 0.02 (6)*	0.88 ± 0.01 (6)*
N92Q/N348Q	0.59 ± 0.02 (6)**	0.80 ± 0.03 (6)*	0.78 ± 0.01 (6)*	0.79 ± 0.02 (6)*
N92Q/N468Q	0.62 ± 0.05 (6)**	0.84 ± 0.02 (6)*	0.80 ± 0.03 (6)*	0.79 ± 0.05 (6)*
N92Q/N594Q	0.74 ± 0.02 (3)**	0.82 ± 0.01 (3)*	0.82 ± 0.01 (3)*	0.80 ± 0.01 (3)*
N92Q/N812Q	0.26 ± 0.01 (3)**	0.54 ± 0.01 (3)**	0.67 ± 0.01 (3)**	0.68 ± 0.01 (3)**
N136Q/N184Q	0.84 ± 0.02 (3)	0.89 ± 0.01 (3)	0.91 ± 0.01 (3)	0.97 ± 0.01 (3)
N136Q/N769Q	1.13 ± 0.02 (3)	0.96 ±0.01 (3)	0.93 ± 0.01 (3)	0.92 ± 0.01 (3)
N348Q/N468Q	0.11 ± 0.01 (3)**	0.47 ± 0.01 (3)**	0.65 ± 0.01 (3)*	0.72 ± 0.01 (3)*
N348Q/N812Q	0.04 ± 0.03 (6)**	0.38 ± 0.01 (6)**	0.55 ± 0.01 (6)**	0.54 ± 0.01 (6)**
N468Q/N812Q	0.16 ± 0.01 (6)**	0.53 ± 0.01 (6)**	0.69 ± 0.01 (6)**	0.76 ± 0.01 (6)**
N594Q/N876Q	0.76 ± 0.03 (3)*	0.82 ± 0.02 (3)*	0.82 ± 0.01 (3)*	0.82 ± 0.02 (3)*
N348Q/N468Q/N812Q	0.04 ± 0.03 (3)**	0.39 ± 0.01 (3)**	0.72 ± 0.01 (3)**	0.74 ± 0.01 (3)**

TABLE 2

Biophysical properties of $Ca_v1.2/Ca_v\beta3$ with $Ca_v\alpha2\delta1$ WT and mutants

$Ca_v1.2$ WT was co-expressed in stable $Ca_v\beta3$ cells with pmCherry-no insert or pmCherry-$Ca_v\alpha2\delta1$-HA WT or mutant using a 1:1 DNA ratio. Biophysical parameters were measured in the presence of 2 mM Ca^{2+} as described elsewhere (17, 22). Activation properties ($E_{0.5,act}$ and ΔG_{act}) were estimated from the mean *I-V* relationships and fitted to a Boltzmann equation. The data are shown with the mean ± S.E. of the individual experiments and the number of experiments appears in parentheses. N.D. not determined because of a poor signal to noise ratio. Statistical analysis was carried out against the values obtained in the presence of mCherry-$Ca_v\alpha2\delta1$-HA WT (* $p < 0.05$; ** $p < 0.01$).

mCherry-$Ca_V\alpha2\delta1$-HA WT or mutant with $Ca_V1.2$ WT in stable $Ca_V\beta3$ cells with 2 mM Ca^{2+}	Biophysical Properties			
	Peak currrent density (pA/pF)	$E_{0.5.act}$ (mV)	ΔG_{act} (kcal mol^{-1})	r100 at +5 mV
empty mCherry vector	-2.6 ± 0.4 (35)**	+8 ± 2 (35)**	+0.5 ± 0.1 (35)**	N.D.
mCherry-$Ca_V\alpha2\delta1$-HA WT	-30 ± 1 (231)	-9.6 ± 0.1 (231)	-0.86 ± 0.02 (231)	0.38 ± 0.02 (231)
N92Q	-20 ± 3 (8)	-6.9 ± 0.6 (8)	-0.61 ± 0.06 (8)	0.26 ± 0.02 (8)
N136Q	-24 ± 6 (8)	-10 ± 1 (8)	-0.9 ± 0.1 (8)	0.26 ± 0.03 (8)
N184Q	-24 ± 5 (8)	-9 ± 1 (8)	-1.0 ± 0.3 (8)	0.32 ± 0.04 (8)
N324Q	-27 ± 5 (11)	-9 ± 1 (11)	-0.9 ± 0.3 (11)	0.30 ± 0.03 (11)
N348Q	-16 ± 3 (18)*	-5 ± 1 (18)*	-0.4 ± 0.1 (18)	0.42 ± 0.03 (18)
N468Q	-21 ± 1 (55)*	-5 ± 1 (55)*	-0.4 ± 0.1 (55)	0.37 ± 0.02 (55)
N585Q	-19 ± 4 (9)*	-10.5 ± 0.8 (9)	-1.5 ± 0.5 (9)	0.30 ± 0.02 (9)
N594Q	-34 ± 5 (8)	-10.3 ± 0.8 (8)	-0.97 ± 0.09 (8)	0.24 ± 0.02 (8)
N663Q	-5 ± 2 (28)**	+3 ± 2 (28)**	+0.1 ± 0.1 (28)**	N.D.
N769Q	-32 ± 6 (8)	-10 ± 1 (8)	-1.0 ± 0.2 (8)	0.32 ± 0.03 (8)
N812Q	-9 ± 2 (30)**	-2 ± 1 (30)**	-0.3 ± 0.1 (30)**	0.44 ± 0.03 (30)**
N876Q	-38 ± 11 (10)	-11 ± 2 (10)	-1.1 ± 0.2 (10)	0.27 ± 0.03 (10)
N986Q	-30 ± 10 (12)	-9 ± 1 (12)	-0.9 ± 0.2 (12)	0.31 ± 0.03 (12)
N92Q/N184Q	-18 ± 4 (10)	-7 ± 1 (10)	-0.6 ± 0.1 (10)	0.34 ± 0.02 (10)
N92Q/N348Q	-11 ± 3 (7)**	-7 ± 1 (7)	-0.53 ± 0.07 (7)	0.36 ± 0.03 (7)
N92Q/N468Q	-13 ± 3 (9)*	-6.1 ± 0.8 (9)	-0.53 ± 0.08 (9)	0.45 ± 0.03 (9)*
N92Q/N594Q	-31 ± 6 (10)	-10 ± 1 (10)	-1.1 ± 0.2 (10)	0.32 ± 0.03 (10)
N92Q/N812Q	-10 ± 5 (8)**	-3 ± 2 (8)**	-0.4 ± 0.1 (8)	0.39 ± 0.03 (8)
N92Q/N876Q	-22 ± 3 (9)	-6 ± 1 (9)	-0.9 ± 0.3 (9)	0.36 ± 0.03 (9)
N136Q/N184Q	-25 ± 5 (17)	-7 ± 1 (17)	-0.5 ± 0.1 (17)	0.32 ± 0.05 (17)
N136Q/N769Q	-27 ± 4 (10)	-7 ± 2 (10)	-0.6 ± 0.2 (10)	0.33 ± 0.04 (10)
N348Q/N468Q	-4 ± 1 (5)**	+2 ± 3 (5)**	+0.1 ± 0.1 (5)**	0.56 ± 0.03 (5)**
N348Q/N812Q	-1.9 ± 0.4 (17)**	+8 ± 2 (17)**	+0.3 ± 0.1 (17)**	0.48 ± 0.08 (17)**
N468Q/N812Q	-3.1 ± 0.9 (6)**	-2 ± 2 (6)*	-0.1 ± 0.1 (6)**	0.44 ± 0.04 (6)**
N594Q/N876Q	-26 ± 6 (10)	-6 ± 1 (10)	-0.6 ± 0.1 (10)	0.31 ± 0.02 (10)
N585Q/N769Q/N883Q	-30 ± 4 (8)	-10 ± 1 (8)	-1.0 ± 0.2 (8)	0.30 ± 0.03 (8)
N92Q/N348Q/N594Q/N876Q	-29 ± 5 (10)	-11 ± 1 (10)	-1.0 ± 0.1 (10)	0.34 ± 0.02 (10)
N585Q/N769Q/N883Q/N1066Q	-35 ± 8 (10)	-10.8 ± 0.4 (10)	-1.1 ± 0.1 (10)	0.28 ± 0.04 (10)
N92Q/N184Q/N468Q/N876Q/N986Q	-19 ± 3 (25)*	-6.6 ± 0.7 (25)	-0.63 ± 0.08 (25)	0.32 ± 0.03 (25)
N92Q/N184Q/N348Q/N594Q/ N812Q/N876Q (6xNQ)	-5 ± 1 (8)**	+1 ± 2 (8)**	-0.2 ± 0.7 (8)**	0.41 ± 0.02 (8)*
N184Q/N348Q/N594Q/ N812Q/N876Q (6xNQ+Q92N)	-8 ± 2 (10)**	-2 ± 1 (10)**	-0.4 ± 0.1 (10)**	0.36 ± 0.01 (10)*
N92Q/N348Q/N594Q/ N812Q/N876Q (6xNQ+Q184N)	-8 ± 2 (10)**	-3 ± 2 (10)**	-0.6 ± 0.1 (10)**	0.36 ± 0.02 (10)
N92Q/N184Q/N594Q/N812Q/ N876Q (6xNQ+Q348N)	-10 ± 4 (17)**	-2 ± 2 (17)**	-0.6 ± 0.8 (17)**	0.38 ± 0.02 (17)
N92Q/N184Q/N348Q/N812Q/ N876Q (6xNQ+Q594N)	-5 ± 2 (10)**	-3 ± 2 (10)**	-0.5 ± 0.1 (10)**	0.30 ± 0.01 (10)
N92Q/N184Q/N348Q/N594Q/ N876Q (6xNQ + Q812N)	-12 ± 2 (19)**	-5.1 ± 0.7 (19)**	-0.41 ± 0.05 (19)**	0.37 ± 0.01 (19)
N92Q/N184Q/N348Q/N594Q/ N812Q (6xNQ+Q876N)	-3.7 ± 0.8 (9)**	+2 ± 2 (9)**	0.0 ± 0.1 (9)**	0.48 ± 0.02 (9)
N92Q/N184Q/N468Q/N594Q/ N876Q/N986Q (6xNQ alt1)	-26 ± 5 (13)	-6 ± 1 (13)	-0.6 ± 0.1 (13)	0.3 ± 0.1 (13)
N92Q/N136Q/N184Q/N348Q/ N468Q/ N585Q/N594Q/N663Q/ N769Q/ N812Q/ N876Q/N883Q/ N986Q/N1066Q (14xNQ)	-1.2 ± 0.2 (5)**	+11 ± 8 (5)**	+0.4 ± 0.3 (5)**	N.D.

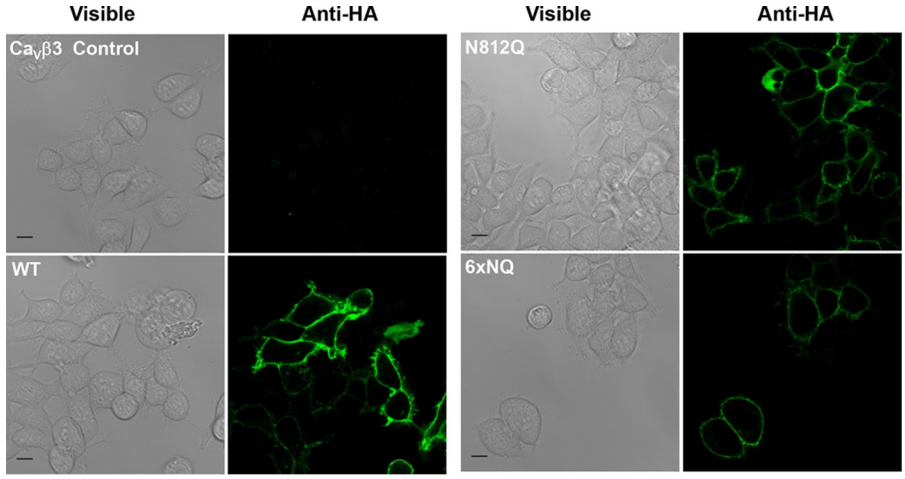

FIGURE 6. **Live cell imaging of $Ca_V\alpha2\delta1$ proteins WT and mutants.** $Ca_V\beta3$ stable HEKT cells were transfected with pCMV-$Ca_V1.2$ and pmCherry-$Ca_V\alpha2\delta1$-HA WT, N812Q, or 6xNQ (N92Q/N184Q/N348Q/N594Q/N812Q/N876Q). One day after transfection, live cells were incubated with the FITC-conjugated anti-HA antibody (1:100) and the nuclei were stained with DAPI (1:1000) (data not shown) in 1× PBS for 45 min at 4 °C. Confocal fluorescent images were captured with a Zeiss LSM 710 confocal microscope system with ×63/1.40 oil objective. *Scale bar* corresponds to 10 μm. The immunofluorescent signals from the FITC-conjugated anti-HA antibody (*green*) are shown to the *right* of the corresponding differential interference contrast images. Under these conditions, the FITC signal was mostly restricted to the cell surface of intact cells. No signal was observed in nontransfected cells (*upper left quadrant*) or in the absence of primary or conjugated antibody (data not shown).

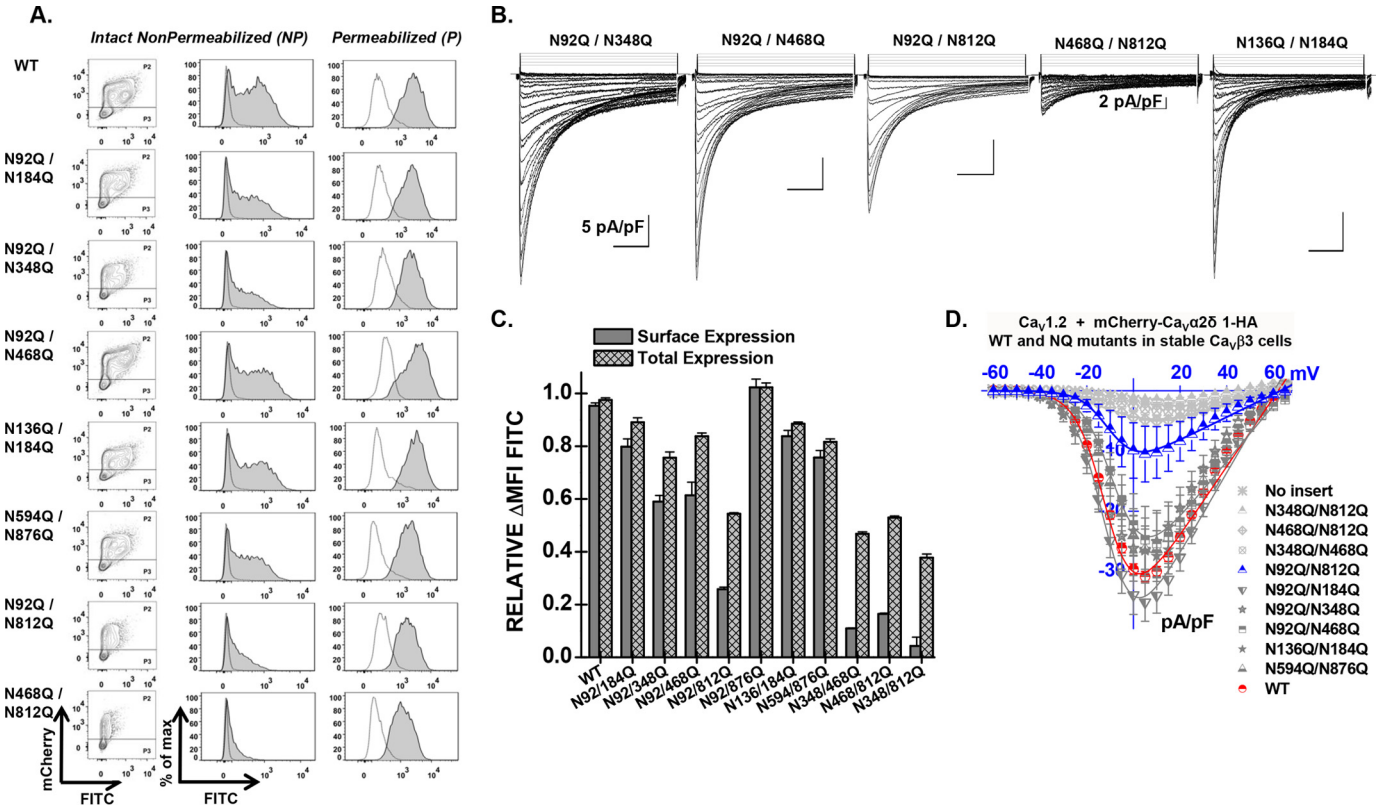

FIGURE 7. **Combining mutations N346Q, N468Q, and N812Q eliminates cell surface expression of $Ca_V\alpha2\delta1$ and modulation of $Ca_V1.2$ whole-cell currents.** *A,* representative two-dimensional plots of mCherry *versus* FITC fluorescence are shown for each mutation as stated. *B,* representative whole-cell Ca^{2+} current traces recorded after recombinant expression of $Ca_V1.2$ in stable $Ca_V\beta3$ cells with mCherry-$Ca_V\alpha2\delta1$-HA WT or some double *N*-glycosylation mutants. Unless specified otherwise, the current density scale is 5 pA/pF. Functional modulation by mCherry-$Ca_V\alpha2\delta1$-HA WT was measured under the same experimental conditions (data not shown). *C, bar graph* shows the normalized ΔMFI measured in the presence of FITC in intact (surface expression) or permeabilized cells (total expression). In all cases, the ΔMFI fluorescence measured for FITC in permeabilized cells was qualitatively similar to the constitutive fluorescence measured for mCherry validating the accessibility of the HA epitope and confirming the values obtained for total protein expression. *D,* current-voltage relationships, recorded in the presence of 2 mM Ca^{2+}, are shown for the double mutations mCherry-$Ca_V\alpha2\delta1$-HA N92Q/N184Q, mCherry-$Ca_V\alpha2\delta1$-HA N92Q/N348Q, mCherry-$Ca_V\alpha2\delta1$-HA N92Q/N468Q, mCherry-$Ca_V\alpha2\delta1$-HA N92Q/N812Q, mCherry-$Ca_V\alpha2\delta1$-HA N348Q/N812Q, mCherry-$Ca_V\alpha2\delta1$-HA N468Q/N812Q, mCherry-$Ca_V\alpha2\delta1$-HA N348Q/N468Q, mCherry-$Ca_V\alpha2\delta1$-HA N594Q/N876Q, and mCherry-$Ca_V\alpha2\delta1$-HA N136Q/N184Q. See Tables 1 and 2 for details.

tively. These results confirm that the simultaneous mutation of these Asn sites significantly affected the glycosylation status of $Ca_V\alpha2\delta1$, although the $Ca_V\alpha2\delta1$ protein remains strongly *N*-linked glycosylated. Together, these data show that the $Ca_V\alpha2\delta1$ protein is heavily glycosylated on many if not all of the 16 Asn sites because the simultaneous mutation

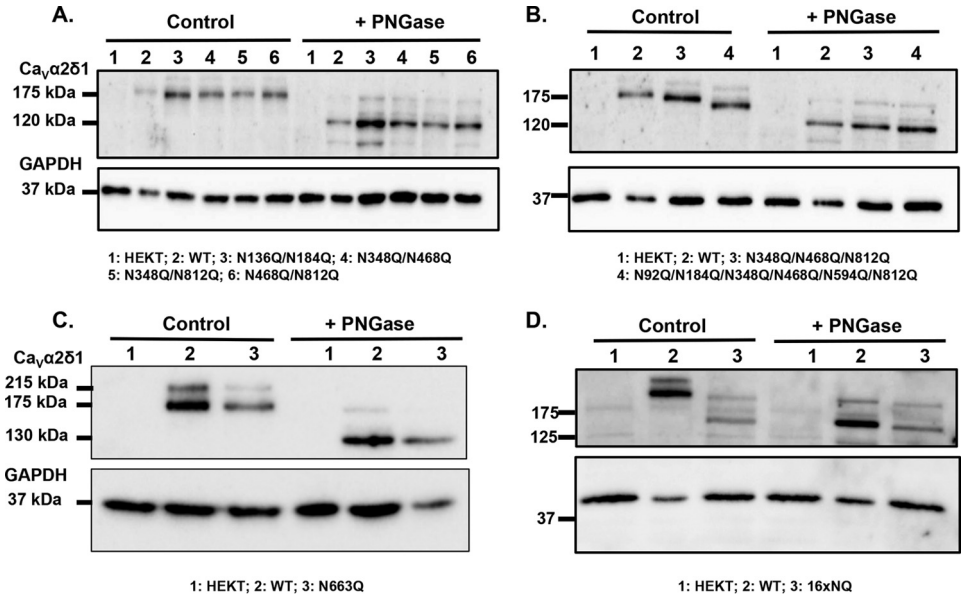

FIGURE 8. **Mutation of all 16 Asn sites appears to eliminate *N*-glycosylation from Ca$_V$α2δ1.** HEKT cells were transiently transfected with pmCherry-Ca$_V$α2δ1-HA WT and mutants as described. One day after transfection, cells were lysed and protein lysates were either treated with the vehicle buffer (control conditions) or with PNGase F. Proteins were fractionated by SDS-PAGE (8%). Western blot analysis was carried out with the Ca$_V$α2δ1 antibody (Alomone Labs) as the primary antibody. *A, lane 1,* mock-transfected HEKT cells; *lane 2,* mCherry-Ca$_V$α2δ1-HA WT; *lane 3,* N136Q/N184Q; *lane 4,* N348Q/N468Q; *lane 5,* N348Q/N812Q; and *lane 6,* N468Q/N812Q. Before treatment with PNGase F, the calculated molecular masses for the high density band were as follows: *lane 2,* 173 kDa; *lane 3,* 163 kDa; *lane 4,* 163 kDa; *lane 5,* 166 kDa; and *lane 6,* 163 kDa. After digestion with PNGase F: *lane 2,* 123 kDa; *lane 3,* 121 kDa; *lane 4,* 121 kDa; *lane 5,* 119 kDa; and *lane 6,* 118 kDa. *Lanes 2* (± *PNGase*) were loaded with 5 μg proteins and *lanes 1; 3–6* (± *PNGase*) were loaded with 10 μg. *B, lane 1,* mock-transfected HEKT cells; *lane 2,* mCherry-Ca$_V$α2δ1-HA WT; *lane 3,* mCherry-Ca$_V$α2δ1-HA N348Q/N468Q/N812Q; and *lane 4,* mCherry-Ca$_V$α2δ1-HA N92Q/N184Q/N348Q/N468Q/N594Q/N812Q. Before PNGase F treatment, the calculated molecular masses for the high density band were as follows: *lane 2,* 173 kDa; *lane 3,* 159 kDa; and *lane 4,* 144 kDa. After digestion with PNGase: *lane 2,* 123 kDa; *lane 3,* 118 kDa; and *lane 4,* 116 kDa. *Lanes 2* (± *PNGase*) were loaded with 5 μg of proteins, and *lanes 1, 3,* and *4* (± *PNGase*) were loaded with 10 μg. *C, lane 1,* mock-transfected HEKT cells; *lane 2,* pmCherry-Ca$_V$α2δ1-HA WT; and *lane 3,* N663Q. Before PNGase F treatment, the calculated molecular masses for the high density band were as follows: *lane 2,* 173 kDa; *lane 3,* 168 kDa. After digestion with PNGase F, the calculated molecular masses for the high density band were as follows: *lane 2,* 130 kDa; *lane 3,* 130 kDa. All lanes were loaded with 10 μg of proteins. *D, lane 1,* mock-transfected HEKT cells; *lane 2,* pmCherry-Ca$_V$α2δ1-HA WT; and *lane 3,* 16xNQ. Before PNGase F treatment, the calculated molecular masses for the high density band were as follows: *lane 2,* 183 kDa; *lane 3,* 132 kDa. After digestion with PNGase F, the calculated molecular masses for the high density band were as follows: *lane 2,* 130 kDa; *lane 3,* 127 kDa. *Lanes 2* (± *PNGase*) were loaded with 10 μg of proteins, and *lanes 1* and *3* were loaded with 20 μg. There was a 50-kDa reduction in the mobility of the recombinant Ca$_V$α2δ1 protein after the simultaneous mutation of the 16 Asn sites. Furthermore, enzymatic deglycosylation with PNGase F produced recombinant Ca$_V$α2δ1 proteins with the same apparent mobility suggesting that the 16 Asn sites account for the complete *N*-glycosylated state of the protein.

of the 16 sites eliminated the formation of the glycosylated protein (Fig. 8*D*).

Protein Stability/Synthesis Was Impaired in Asn Mutants—The decrease in the cell surface density of the double mutants N348Q/N812Q and N468Q/N812Q was accompanied by a 50–60% decrease in the FITC fluorescence under permeabilized conditions suggesting that protein stability was severely altered. Chase assays were carried out in the presence of cycloheximide (a blocker of *de novo* protein synthesis) to document the time course of protein degradation. Cycloheximide was added 24 h after transfection, and total cell lysates were collected at different time points. Protein density was estimated from Western blots relative to the loading control GAPDH and normalized using the protein density of the WT construct at time 0 (Fig. 9, *A–C*). In all cases, the major band formed by the mCherry-Ca$_V$α2δ1-HA WT construct disappeared with a half-life estimated at 2.8 ± 0.5 h ($n = 7$) (Fig. 9*D*). As compared with the WT construct, the relative protein density of the double mutants N348Q/N812Q and N468Q/N812Q were significantly lower even at time 0. The degradation kinetics were also slightly faster with $t_{½} \approx 1.2 \pm 0.8$ h ($n = 2$) and $t_{½} = 1.8 \pm 0.5$ h ($n = 3$), respectively. These data suggest that *N*-glycosylation at these sites is required for protein translation or else that kinetics of degradation of NQ mutants are faster than the kinetics of protein synthesis, an observation that was also reported for glycosylation-defective mutations of the type 1 transmembrane auxiliary subunit KCNE1 (43).

Discussion

16 Asn Sites Account for N-type Glycosylation of Ca$_V$α2δ1—*N*-Linked glycosylation is one of the most common post-translational modifications known to influence the turnover and the stability of cardiac ion channels (61–65). With the cardiac Ca$_V$1.2 macromolecular complex, Ca$_V$α2δ1 is the most heavily glycosylated protein (13) with *N*-glycans increasing the apparent molecular mass by about 50 kDa. The fully glycosylated form was found to be the dominant protein species of the endogenous Ca$_V$α2δ1 found in the plasma and associated caveolae membranes of isolated cardiomyocytes. In this work, we have addressed the role of *N*-glycosylation in the protein density, steady-state cell surface levels, and the function of the Ca$_V$α2δ1 auxiliary subunit using mobility shift assays, cycloheximide pulse-chase analysis, flow cytometry assays, and patch clamp recordings of recombinant Ca$_V$1.2 currents. The 16 consensus N-type glycosylation sites were characterized after single or multiple mutations of Asn to Gln. By combining fluorescence and functional assays, we demonstrated that multiple glycosylation-defective mutants reduced the steady-state

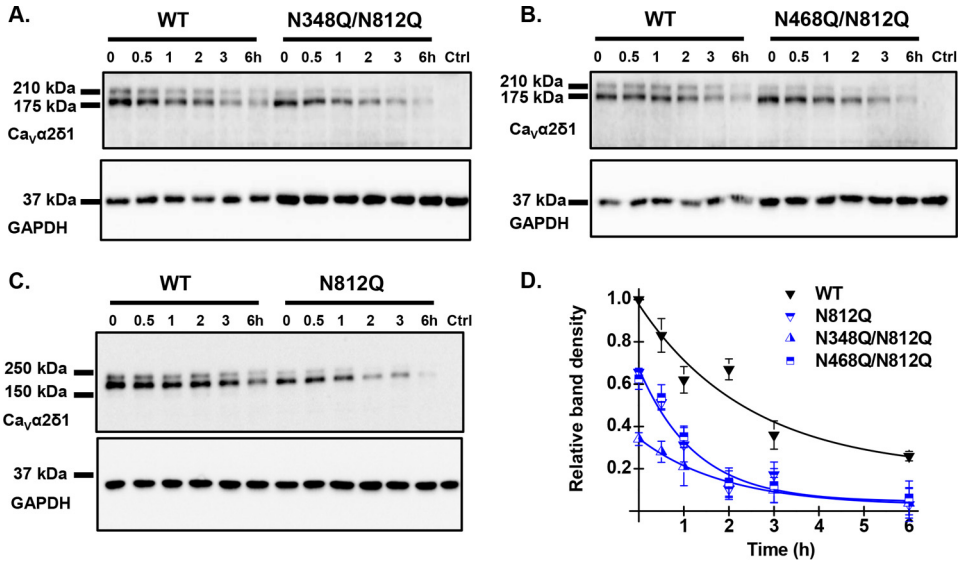

FIGURE 9. **Multiple Asn mutations may impair protein stability.** HEKT cells were transiently transfected with pmCherry-Ca$_V$α2δ1-HA WT and the glycosylation mutants N348Q/N812Q (*A*), N468Q/N812Q (*B*), and N812Q (*C*). Exactly 24 h after transfection, subconfluent cells were incubated with 100 μg/ml cycloheximide. At the indicated time points, cell lysates were prepared and fractionated by SDS-PAGE (8%). Ca$_V$α2δ1 and GAPDH proteins were respectively probed with anti-Ca$_V$α2δ1 (Alomone Labs) and anti-GAPDH. Please note that we loaded 2× more proteins in the wells for the double mutants to visualize their time course alongside the WT construct. In particular, each lane for Ca$_V$α2δ1-HA WT was loaded with 5 μg of proteins in *A* and *B*, and 10 μg of proteins were loaded for N348Q/N812Q and N468Q/N812Q. *C*, 10 μg of proteins were loaded for Ca$_V$α2δ1-HA WT and N812Q. *D*, protein density was estimated relative to the density of the GAPDH band and normalized to the protein density for the wild-type construct at time 0. Protein band intensities were quantified by densitometry using ImageLab (Bio-Rad) software at a single exposure selected for clear bands without saturation. Averaged data points were fitted with a mono-exponential decay function. The half-life was $t_{1/2} = 2.8 \pm 0.5$ h ($n = 7$) for pmCherry-Ca$_V$α2δ1-HA WT; $t_{1/2} = 1.2 \pm 0.8$ h ($n = 2$) for N348Q/N812Q; $t_{1/2} = 1.8 \pm 0.5$ h ($n = 3$) for N468Q/N812Q; and $t_{1/2} = 1.9 \pm 0.7$ h ($n = 3$) for N812Q. As seen, the data points for the decay of N812Q and N468Q/N812Q are superimposed with similar relative densities, whereas protein density for N348Q/N812Q was lower at time 0.

cell surface density, decreased total protein density, and diminished protein stability of Ca$_V$α2δ1. The drop in the cell surface expression of Ca$_V$α2δ1 in turn significantly impaired peak current density and activation gating of the L-type Ca$_V$1.2 channel.

Enzymatic digestion with PNGase F of the native and recombinant Ca$_V$α2δ1 reduced by 50 kDa the electrophoretic mobility of the protein. A similar mobility shift was observed when comparing the migration profile of the WT and the 16xNQ construct demonstrating that many if not all the 16 Asn sites are required to account for the *N*-glycosylated state of the Ca$_V$α2δ1 protein. Interestingly, the recently published three-dimensional structure of the skeletal muscle Ca$_V$1.1 channel complex is compatible with the proposition that most 16 *N*-glycan sites are glycosylated (66). The nature of the carbohydrate chain modifications that the protein undergoes from the endoplasmic reticulum to the post-Golgi compartments was not investigated in this work. We used throughout PNGase F, an amidase that cleaves between the innermost *N*-acetylglucosamine and Asn residues of high mannose, hybrid, and complex oligosaccharides from *N*-linked glycoproteins, thus stripping all glycans from the protein. Protein biogenesis further includes trimming of glucose and mannose residues by glycosidases and addition of new residues via glycosyltransferases in the ER and, to a great extent, in the Golgi. In the Golgi, high mannose *N*-glycans can be converted to a variety of complex and hybrid forms that are unique to each protein (67). The Ca$_V$α2δ1 protein thus contains multiple glycosylation sites that may be modified with any of the three classes of *N*-linked glycans. Adding to the complexity, different units of the same Ca$_V$α2δ1 glycoprotein may have different glycan structures attached to the identical Asn site. From the mobility shift assays conducted with the multiple mutants, it can be argued that many of these 16 sequons are modified by *N*-glycans even N*X*S sequons with negatively charged or hydrophobic amino acids at the *X*-position (such as Asn-136 and Asn-184) that are considered to be poorer substrates for the oligosaccharyltransferase complex (43, 56). The *N*-glycan modification of many sequons appears to individually contribute 3–5 kDa to Ca$_V$α2δ1. Although this is often difficult to detect visually for single mutations, it can be seen more clearly with double mutants.

Mutation of Asn-663 Prevents Cell Surface Density of Ca$_V$α2δ1—The single mutation of Asn-663 (N663Q) prevented the detection of the protein at the cell surface by immunofluorescence and channel modulation. Asn-663 is located close to the 9-residue HA epitope that was inserted after Asp-676 in the primary structure of Ca$_V$α2δ1. However, substitution of the asparagine for the glutamine residue did not prevent protein synthesis as the protein was expressed with the expected molecular mass. Furthermore, the mCherry and the HA epitope of this construction were fluorescently labeled and detected in intact and permeabilized cells, respectively. Every other single Asn mutation within the 16 sites did not significantly affect cell surface density or protein function thus making Asn-663 one of the most critical single sites for protein expression. Asn sites in the 6xNQ mutant prevented protein detection at the surface and impaired modulation of Ca$_V$1.2 currents. Double mutations pairing N348Q, N812Q, and/or N468Q were sufficient to prevent the detection of Ca$_V$α2δ1 at the cell surface and abolished the subunit-mediated stimulation of Ca$_V$1.2 currents. Other double Asn mutations, including the N136Q/N184Q mutant (60), did not affect cell surface density or protein function. One reason for this discrepancy may lie

in the differences in the mode of regulation of $Ca_V1.2$ and $Ca_V2.2$ channels by $Ca_V\alpha2\delta1$. To limit the number of double mutants to be tested (120 possible double mutants for 16 sequons), our strategy was to produce and characterize multiple mutants that impacted on channel function. Multiple mutants produced with either N348Q, N468Q, or N812Q showed a significant decrease in cell surface density and protein function, whereas every single mutation pairing N663Q was not functional. It is impossible to know at this time whether *N*-glycans at these sites interact with each other or with the pore-forming subunit. Current algorithms and the recent three-dimensional structure of the skeletal $Ca_V1.1$ channel complex (66) are identifying important structural domains but are not predicting the spatial orientation of the 16 *N*-glycans with each other and other proteins in the channel.

Protein Stability Was Decreased in Glycosylation-defective Mutants of $Ca_V\alpha2\delta1$—The molecular and cellular pathways responsible for the compromised steady-state cell surface expression of the glycosylation-defective $Ca_V\alpha2\delta1$ proteins remain to be fully elucidated. The decreased surface levels could result from impaired translational rate (68, 69), ER folding yield, trans-Golgi cargo sorting, increased degradation, and/or a combination of these processes. The relative contribution of lectin chaperones, such as calnexin and calreticulin, to protein biogenesis and the nature of the key enzymes responsible for degradation within the ubiquitin-proteasome system of ERAD (68, 70–72) also remain to be identified. Outstanding issues include the identification of the quality control networks that are affected by these specific glycosylation sites (73, 74) and the potential cross-talk between ERAD and autophagy, the two major cellular degradative pathways (75). Finally, there is always the question of overexpressing cardiac proteins in a model cell to study translation events. These are important questions that currently go beyond the scope of this work. Protein assays herein reported nonetheless support the view that protein stability and/or protein synthesis was impaired in Asn mutants suggesting that *N*-glycosylation is a co-translational event (43). The observation that partially glycosylated forms of $Ca_V\alpha2\delta1$ were notably absent from whole-cell homogenates prepared with recombinant cells as well as isolated cardiomyocytes further argues for this scenario.

L-type Channel Modulation by $Ca_V\alpha2\delta1$—Up-regulation of L-type currents requires robust cell surface density of $Ca_V\alpha2\delta1$ in cardiomyocytes (19) and in HEKT cells (22). Alterations in the cell surface density of $Ca_V\alpha2\delta1$ caused by mutating glycosylation sites (our study), arrhythmogenic mutations (22), mutations within the "von Willebrand factor" structural domain (76, 77), or following pharmacological modulation (*e.g.* gabapentin) (76, 78, 79) were shown to decrease channel function by altering the surface levels of $Ca_V\alpha2\delta1$ (76, 77). With the exception of the so-called R-domain (80), these manipulations altered the function of $Ca_V\alpha2\delta1$ (and by extension the function of voltage-gated currents) through a decrease in the membrane expression of $Ca_V\alpha2\delta1$. By analogy with other type 1 transmembrane regulatory subunits of voltage-gated ion channels, $Ca_V\alpha2\delta1$ could interact with the pore-forming subunit either within the membrane through the voltage sensing domain (as KCNE with Kv7/KCNQ1 channel (81)) and/or from the external portion of the protein by interacting with the external pore domain (77). The optimal ratio for channel modulation remains to be established. By comparison, a single high affinity intracellular binding site for $Ca_V\beta$ onto the I-II linker of the $Ca_V\alpha1$ subunit from high voltage-activated Ca_V1 and Ca_V2 channels has been identified (17, 46, 82–84). Whether a single $Ca_V\alpha2\delta1$ subunit could interact with two $Ca_V\alpha1$ or whether the L-type $Ca_V1.2$ channel complex (85) can accommodate two or more $Ca_V\alpha2\delta1$ subunits remains a question for debate. Nonetheless, mutations affecting the expression of $Ca_V\alpha2\delta1$ is likely to influence Ca^{2+} balance in cardiomyocytes (86–88) as in arterial smooth muscle cells (4) by virtue of controlling the activity of L-type $Ca_V1.2$ channels (22).

Recent technical advances in glycoprotein crystallography suggest that the more mobile *N*-glycans on cell surface receptors could guide the partner ligand to its binding site and prevent irregular protein aggregation by covering oligomerization sites away from the ligand-binding site (91). Beyond their role in protein biogenesis and/or stability (37), *N*-linked glycans promote interactions with cell adhesion proteins and signaling molecules (40, 89) as it is widely understood for members of the integrin family (90). Glycans could also contribute to channel modulation by altering the surface potential sensed by the gating machinery (92) and/or by modifying conformational changes regulating cooperative subunit interactions during channel activation (93). The Asn-812 site is a choice candidate for such a mechanism. The N812Q mutant was expressed at the cell surface to the same extent as 4xNQ mutant, yet it caused a more extensive decrease in channel function. It can be speculated that *N*-glycans at the Asn-812 site contribute to the functional interaction with the pore-forming subunit of the $Ca_V1.2$ channel, either through direct protein-protein interaction and/or by promoting a favorable gating conformation (31). Most structural models predict that the extracellular domain is quite disordered, making it impossible to predict the relative orientation and/or interaction of each *N*-glycan chain within the $Ca_V1.2$ channel complex. The nature of the protein-protein interaction (either direct or through a secondary partner), the sites responsible for this interaction, and well as the affinity of the interaction will await further structural characterization of the cardiac $Ca_V1.2$ channels. At this time, three-dimensional structures of the purified cardiac $Ca_V1.2$ channel complex position the extracellular portion of $Ca_V\alpha2\delta1$ on top of the channel complex at a resolution that prevents identifying interaction domains (32), although the recent three-dimensional structure of the skeletal muscle $Ca_V1.1$ channel complex suggests that the VWA domain in $Ca_V\alpha2\delta1$ may be directly interacting with the voltage-sensing region of the pore-forming $Ca_V\alpha1$ subunit (66). Nonetheless, it is becoming quite evident that biological networks exploit cell-surface glycans to coordinate membrane protein complexes (94). Defects in the glycosylation of type I transmembrane auxiliary subunit $Ca_V\alpha2\delta1$ could hence trigger ventricular and atrial arrhythmias (22, 95) by decreasing the fraction of functional L-type $Ca_V1.2$ channels. Hence, elucidating the cellular processes controlled by glycosylation contributes to furthering our understanding of most biological systems and, in particular, voltage-gated cardiac ion channels.

Author Contributions—M. P. T. produced the single and multiple Asn mutants, performed and analyzed the vast majority of the flow cytometry experiments, carried out the cycloheximide chase assays, and stained the HEKT cells for confocal microscopy. B. B. isolated the mouse cardiomyocytes, conducted patch clamp experiments, isolated the sarcolemmal membrane fractions from mouse cardiomyocytes and the plasma membrane fraction from recombinant HEKT cells, as well as carried out the Western blots in Fig. 1*B* and Fig. 2*A*. J. B. produced some constructs, and performed the experiments shown in Fig. 2*C*. E. S. conducted flow cytometry and patch clamp experiments for a few mutants. S. L. supervised the analysis of the flow cytometry experiments. C. F. supervised the isolation and the culture of the mouse cardiomyocytes. L. P. designed and coordinated the study, interpreted the data, and wrote the manuscript. All authors reviewed the results and approved the final version of this manuscript.

Acknowledgments—We thank Serge Sénéchal and Dr. Jacques Thibodeau for sharing their expertise and for granting us access to their flow cytometry and cell sorting platform; Behzad Shakeri and Dr. Guillaume Roussel for contribution to patch clamp recordings; Louis Villeneuve for invaluable assistance in confocal microscopy; Nathalie Ethier for help in isolating adult mouse hearts; Julie Verner for superb training in cell culture methods; and Dr. Rémy Sauvé for critical reading of the manuscript.

References

1. Richard, S., Perrier, E., Fauconnier, J., Perrier, R., Pereira, L., Gõmez, A. M., and Bénitah, J. P. (2006) Calcium-induced calcium entry or how the L-type calcium channel remodels its own signalling pathway in cardiac cells. *Prog. Biophys. Mol. Biol.* **90,** 118–135
2. Bers, D. M. (2000) Calcium fluxes involved in control of cardiac myocyte contraction. *Circ. Res.* **87,** 275–281
3. Kamp, T. J., and Hell, J. W. (2000) Regulation of cardiac L-type calcium channels by protein kinase A and protein kinase C. *Circ. Res.* **87,** 1095–1102
4. Bannister, J. P., Bulley, S., Narayanan, D., Thomas-Gatewood, C., Luzny, P., Pachuau, J., and Jaggar, J. H. (2012) Transcriptional upregulation of $\alpha 2\delta 1$ elevates arterial smooth muscle cell voltage-dependent Ca^{2+} channel surface expression and cerebrovascular constriction in genetic hypertension. *Hypertension* **60,** 1006–1015
5. Yue, L., Feng, J., Gaspo, R., Li, G. R., Wang, Z., and Nattel, S. (1997) Ionic remodeling underlying action potential changes in a canine model of atrial fibrillation. *Circ. Res.* **81,** 512–525
6. Van Wagoner, D. R., Pond, A. L., Lamorgese, M., Rossie, S. S., McCarthy, P. M., and Nerbonne, J. M. (1999) Atrial L-type calcium currents and human atrial fibrillation. *Circ. Res.* **85,** 428–436
7. Aschar-Sobbi, R., Izaddoustdar, F., Korogyi, A. S., Wang, Q., Farman, G. P., Yang, F., Yang, W., Dorian, D., Simpson, J. A., Tuomi, J. M., Jones, D. L., Nanthakumar, K., Cox, B., Wehrens, X. H., Dorian, P., and Backx, P. H. (2015) Increased atrial arrhythmia susceptibility induced by intense endurance exercise in mice requires TNFα. *Nat. Commun.* **6,** 6018
8. Lugenbiel, P., Wenz, F., Govorov, K., Schweizer, P. A., Katus, H. A., and Thomas, D. (2015) Atrial fibrillation complicated by heart failure induces distinct remodeling of calcium cycling proteins. *PLoS ONE* **10,** e0116395
9. Richard, S., Leclercq, F., Lemaire, S., Piot, C., and Nargeot, J. (1998) Calcium currents in compensated hypertrophy and heart failure. *Cardiovasc. Res.* **37,** 300–311
10. Mukherjee, R., and Spinale, F. G. (1998) L-type calcium channel abundance and function with cardiac hypertrophy and failure: a review. *J. Mol. Cell. Cardiol.* **30,** 1899–1916
11. Catterall, W. A. (2000) Structure and regulation of voltage-gated Ca^{2+} channels. *Annu. Rev. Cell Dev. Biol.* **16,** 521–555
12. Peterson, B. Z., DeMaria, C. D., Adelman, J. P., and Yue, D. T. (1999) Calmodulin is the Ca^{2+} sensor for Ca^{2+}-dependent inactivation of L-type calcium channels. *Neuron* **22,** 549–558
13. Dolphin, A. C. (2009) Calcium channel diversity: multiple roles of calcium channel subunits. *Curr. Opin. Neurobiol.* **19,** 237–244
14. Dai, S., Hall, D. D., and Hell, J. W. (2009) Supramolecular assemblies and localized regulation of voltage-gated ion channels. *Physiol. Rev.* **89,** 411–452
15. Gao, T., Puri, T. S., Gerhardstein, B. L., Chien, A. J., Green, R. D., and Hosey, M. M. (1997) Identification and subcellular localization of the subunits of L-type calcium channels and adenylyl cyclase in cardiac myocytes. *J. Biol. Chem.* **272,** 19401–19407
16. Carl, S. L., Felix, K., Caswell, A. H., Brandt, N. R., Ball, W. J., Jr., Vaghy, P. L., Meissner, G., and Ferguson, D. G. (1995) Immunolocalization of sarcolemmal dihydropyridine receptor and sarcoplasmic reticular triadin and ryanodine receptor in rabbit ventricle and atrium. *J. Cell Biol.* **129,** 673–682
17. Bourdin, B., Marger, F., Wall-Lacelle, S., Schneider, T., Klein, H., Sauvé, R., and Parent, L. (2010) Molecular determinants of the Cavβ-induced plasma membrane targeting of the Cav1.2 channel. *J. Biol. Chem.* **285,** 22853–22863
18. Altier, C., Garcia-Caballero, A., Simms, B., You, H., Chen, L., Walcher, J., Tedford, H. W., Hermosilla, T., and Zamponi, G. W. (2011) The Cav[β] subunit prevents RFP2-mediated ubiquitination and proteasomal degradation of L-type channels. *Nat. Neurosci.* **14,** 173–180
19. Fuller-Bicer, G. A., Varadi, G., Koch, S. E., Ishii, M., Bodi, I., Kadeer, N., Muth, J. N., Mikala, G., Petrashevskaya, N. N., Jordan, M. A., Zhang, S. P., Qin, N., Flores, C. M., Isaacsohn, I., Varadi, M., *et al.* (2009) Targeted disruption of the voltage-dependent calcium channel $\alpha 2/\delta 1$ subunit. *Am. J. Physiol. Heart Circ. Physiol* **297,** H117–H124
20. Singer, D., Biel, M., Lotan, I., Flockerzi, V., Hofmann, F., and Dascal, N. (1991) The roles of the subunits in the function of the calcium channel. *Science* **253,** 1553–1557
21. Parent, L., Schneider, T., Moore, C. P., and Talwar, D. (1997) Subunit regulation of the humain brain α_{1E} calcium channel. *J. Membr. Biol.* **160,** 127–140
22. Bourdin, B., Shakeri, B., Tétreault, M. P., Sauvé, R., Lesage, S., and Parent, L. (2015) Functional characterization of CaVa2d mutations associated with sudden cardiac death. *J. Biol. Chem.* **290,** 2854–2869
23. Yasuda, T., Chen, L., Barr, W., McRory, J. E., Lewis, R. J., Adams, D. J., and Zamponi, G. W. (2004) Auxiliary subunit regulation of high-voltage activated calcium channels expressed in mammalian cells. *Eur. J. Neurosci.* **20,** 1–13
24. Dolphin, A. C. (2013) The $\alpha 2\delta$ subunits of voltage-gated calcium channels. *Biochim. Biophys. Acta* **1828,** 1541–1549
25. Chang, F. C., and Hosey, M. M. (1988) Dihydropyridine and phenylalkylamine receptors associated with cardiac and skeletal muscle calcium channels are structurally different. *J. Biol. Chem.* **263,** 18929–18937
26. Marais, E., Klugbauer, N., and Hofmann, F. (2001) Calcium channel $\alpha 2\delta$ subunits: structure and gabapentin binding. *Mol. Pharmacol.* **59,** 1243–1248
27. Jay, S. D., Sharp, A. H., Kahl, S. D., Vedvick, T. S., Harpold, M. M., and Campbell, K. P. (1991) Structural characterization of the dihydropyridine-sensitive calcium channel α_2-subunit and the associated δ peptides. *J. Biol. Chem.* **266,** 3287–3293
28. Andrade, A., Sandoval, A., Oviedo, N., De Waard, M., Elias, D., and Felix, R. (2007) Proteolytic cleavage of the voltage-gated Ca^{2+} channel $\alpha 2\delta$ subunit: structural and functional features. *Eur. J. Neurosci.* **25,** 1705–1710
29. Davies, A., Kadurin, I., Alvarez-Laviada, A., Douglas, L., Nieto-Rostro, M., Bauer, C. S., Pratt, W. S., and Dolphin, A. C. (2010) The $\alpha 2\delta$ subunits of voltage-gated calcium channels form GPI-anchored proteins, a posttranslational modification essential for function. *Proc. Natl. Acad. Sci. U.S.A.* **107,** 1654–1659
30. Robinson, P., Etheridge, S., Song, L., Shah, R., Fitzgerald, E. M., and Jones, O. T. (2011) Targeting of voltage-gated calcium channel $\alpha 2\delta$-1 subunit to lipid rafts is independent from a GPI-anchoring motif. *PLoS ONE* **6,** e19802
31. Gurnett, C. A., De Waard, M., and Campbell, K. P. (1996) Dual function of the voltage-dependent calcium channel $\alpha 2\delta$ subunit in current stimula-

tion and subunit interaction. *Neuron* **16,** 431–440
32. Walsh, C. P., Davies, A., Butcher, A. J., Dolphin, A. C., and Kitmitto, A. (2009) Three-dimensional structure of CaV3.1. *J. Biol. Chem.* **284,** 22310–22321
33. Markkanen, P. M., and Petäjä-Repo, U. E. (2008) *N*-Glycan-mediated quality control in the endoplasmic reticulum is required for the expression of correctly folded δ-opioid receptors at the cell surface. *J. Biol. Chem.* **283,** 29086–29098
34. Weng, T. Y., Chiu, W. T., Liu, H. S., Cheng, H. C., Shen, M. R., Mount, D. B., and Chou, C. Y. (2013) Glycosylation regulates the function and membrane localization of KCC4. *Biochim. Biophys. Acta* **1833,** 1133–1146
35. Lu, J., Robinson, J. M., Edwards, D., and Deutsch, C. (2001) T1-T1 interactions occur in ER membranes while nascent Kv peptides are still attached to ribosomes. *Biochemistry* **40,** 10934–10946
36. Vacher, H., and Trimmer, J. S. (2012) Trafficking mechanisms underlying neuronal voltage-gated ion channel localization at the axon initial segment. *Epilepsia* **53,** 21–31
37. Scott, H., and Panin, V. M. (2014) The role of protein *N*-glycosylation in neural transmission. *Glycobiology* **24,** 407–417
38. Aebi, M., Bernasconi, R., Clerc, S., and Molinari, M. (2010) *N*-Glycan structures: recognition and processing in the ER. *Trends Biochem. Sci.* **35,** 74–82
39. Ioffe, E., and Stanley, P. (1994) Mice lacking *N*-acetylglucosaminyltransferase I activity die at mid-gestation, revealing an essential role for complex or hybrid *N*-linked carbohydrates. *Proc. Natl. Acad. Sci. U.S.A.* **91,** 728–732
40. Dennis, J. W., Nabi, I. R., and Demetriou, M. (2009) Metabolism, cell surface organization, and disease. *Cell* **139,** 1229–1241
41. Park, K. H., Kwok, S. M., Sharon, C., Baerga, R., Berga, R., and Sesti, F. (2003) *N*-Glycosylation-dependent block is a novel mechanism for drug-induced cardiac arrhythmia. *FASEB J.* **17,** 2308–2309
42. Schulze-Bahr, E., Wang, Q., Wedekind, H., Haverkamp, W., Chen, Q., Sun, Y., Rubie, C., Hördt, M., Towbin, J. A., Borggrefe, M., Assmann, G., Qu, X., Somberg, J. C., Breithardt, G., Oberti, C., and Funke, H. (1997) KCNE1 mutations cause jervell and Lange-Nielsen syndrome. *Nat. Genet.* **17,** 267–268
43. Bas, T., Gao, G. Y., Lvov, A., Chandrasekhar, K. D., Gilmore, R., and Kobertz, W. R. (2011) Post-translational *N*-glycosylation of type I transmembrane KCNE1 peptides: implications for membrane protein biogenesis and disease. *J. Biol. Chem.* **286,** 28150–28159
44. Du, D., Yang, H., Norring, S. A., and Bennett, E. S. (2014) *In-silico* modeling of glycosylation modulation dynamics in hERG ion channels and cardiac electrical signals. *IEEE J. Biomed. Health Inform.* **18,** 205–214
45. Castellano, A., Wei, X., Birnbaumer, L., and Perez-Reyes, E. (1993) Cloning and expression of a third calcium channel β subunit. *J. Biol. Chem.* **268,** 3450–3455
46. Shakeri, B., Bourdin, B., Demers-Giroux, P. O., Sauvé, R., and Parent, L. (2012) A quartet of leucine residues in the guanylate kinase domain of CaVβ determines the plasma membrane density of the CaV2.3 channel. *J. Biol. Chem.* **287,** 32835–32847
47. Williams, M. E., Feldman, D. H., McCue, A. F., Brenner, R., Velicelebi, G., Ellis, S. B., and Harpold, M. M. (1992) Structure and functional expression of α_1, α_2, and β subunits of a novel human neuronal calcium channel subtype. *Neuron* **8,** 71–84
48. Grandy, S. A., Trépanier-Boulay, V., and Fiset, C. (2007) Postnatal development has a marked effect on ventricular repolarization in mice. *Am. J. Physiol. Heart Circ. Physiol* **293,** H2168–H2177
49. Trépanier-Boulay, V., Lupien, M. A., St-Michel, C., and Fiset, C. (2004) Postnatal development of atrial repolarization in the mouse. *Cardiovasc. Res.* **64,** 84–93
50. Lizotte, E., Tremblay, A., Allen, B. G., and Fiset, C. (2005) Isolation and characterization of subcellular protein fractions from mouse heart. *Anal. Biochem.* **345,** 47–54
51. Lee, G. H., Badorff, C., and Knowlton, K. U. (2000) Dissociation of sarcoglycans and the dystrophin carboxyl terminus from the sarcolemma in enteroviral cardiomyopathy. *Circ. Res.* **87,** 489–495
52. Clark, R. B., Tremblay, A., Melnyk, P., Allen, B. G., Giles, W. R., and Fiset, C. (2001) T-tubule localization of the inward-rectifier K(+) channel in mouse ventricular myocytes: a role in K^+ accumulation. *J. Physiol.* **537,** 979–992
53. Wall-Lacelle, S., Hossain, M. I., Sauvé, R., Blunck, R., and Parent, L. (2011) Double mutant cycle analysis identified a critical leucine residue in IIS4-S5 linker for the activation of the Cav2.3 calcium channel. *J. Biol. Chem.* **286,** 27197–27205
54. Yifrach, O., and MacKinnon, R. (2002) Energetics of pore opening in a voltage-gated K^+ channel. *Cell* **111,** 231–239
55. Stanley, P., Schachter, H., and Taniguchi, N. (2009) in *Essentials of Glycobiology* (Varki, A., Cummings, R. D., Esko, J. D., Freeze, H. H., Stanley, P., Bertozzi, C. R., Hart, G. W., and Etzler, M. E., eds) 2nd Ed., Cold Spring Harbor Laboratory Press, Cold Spring Harbor, New York
56. Kasturi, L., Chen, H., and Shakin-Eshleman, S. H. (1997) Regulation of *N*-linked core glycosylation: use of a site-directed mutagenesis approach to identify Asn-Xaa-Ser/Thr sequons that are poor oligosaccharide acceptors. *Biochem. J.* **323,** 415–419
57. Douglas, L., Davies, A., Wratten, J., and Dolphin, A. C. (2006) Do voltage-gated calcium channel α2δ subunits require proteolytic processing into α2 and δ to be functional? *Biochem. Soc. Trans.* **34,** 894–898
58. Davies, A., Douglas, L., Hendrich, J., Wratten, J., Tran Van Minh, A., Foucault, I., Koch, D., Pratt, W. S., Saibil, H. R., and Dolphin, A. C. (2006) The calcium channel α2δ2 subunit partitions with Cav2.1 into lipid rafts in cerebellum: implications for localization and function. *J. Neurosci.* **26,** 8748–8757
59. Blom, N., Sicheritz-Pontén, T., Gupta, R., Gammeltoft, S., and Brunak, S. (2004) Prediction of post-translational glycosylation and phosphorylation of proteins from the amino acid sequence. *Proteomics* **4,** 1633–1649
60. Sandoval, A., Oviedo, N., Andrade, A., and Felix, R. (2004) Glycosylation of asparagines 136 and 184 is necessary for the α2δ subunit-mediated regulation of voltage-gated calcium channels. *FEBS Lett.* **576,** 21–26
61. Petrecca, K., Atanasiu, R., Akhavan, A., and Shrier, A. (1999) *N*-Linked glycosylation sites determine HERG channel surface membrane expression. *J. Physiol.* **515,** 41–48
62. Gong, Q., Anderson, C. L., January, C. T., and Zhou, Z. (2002) Role of glycosylation in cell surface expression and stability of HERG potassium channels. *Am. J. Physiol. Heart Circ. Physiol.* **283,** H77–H84
63. Cohen, S. A., and Levitt, L. K. (1993) Partial characterization of the rH1 sodium channel protein from rat heart using subtype-specific antibodies. *Circ. Res.* **73,** 735–742
64. Laedermann, C. J., Syam, N., Pertin, M., Decosterd, I., and Abriel, H. (2013) β1- and β3-voltage-gated sodium channel subunits modulate cell surface expression and glycosylation of Nav1.7 in HEK293 cells. *Front. Cell. Neurosci.* **7**, 137
65. Mercier, A., Clément, R., Harnois, T., Bourmeyster, N., Bois, P., and Chatelier, A. (2015) Nav1.5 channels can reach the plasma membrane through distinct *N*-glycosylation states. *Biochim. Biophys. Acta* **1850,** 1215–1223
66. Wu, J., Yan, Z., Li, Z., Yan, C., Lu, S., Dong, M., and Yan, N. (2015) Structure of the voltage-gated calcium channel Cav1.1 complex. *Science* **350,** 10.1126/science.aad2395
67. Freeze, H. H., and Kranz, C. (2010) Endoglycosidase and glycoamidase release of *N*-linked glycans. *Curr. Protoc. Protein Sci.* Chapter 12, Unit 12.4
68. Glozman, R., Okiyoneda, T., Mulvihill, C. M., Rini, J. M., Barriere, H., and Lukacs, G. L. (2009) *N*-Glycans are direct determinants of CFTR folding and stability in secretory and endocytic membrane traffic. *J. Cell Biol.* **184,** 847–862
69. Muthusamy, S., Malhotra, P., Hosameddin, M., Dudeja, A. K., Borthakur, S., Saksena, S., Gill, R. K., Dudeja, P. K., and Alrefai, W. A. (2015) *N*-Glycosylation is essential for ileal ASBT function and protection against proteases. *Am. J. Physiol. Cell Physiol.* **308,** C964–C971
70. Rougier, J. S., Albesa, M., Syam, N., Halet, G., Abriel, H., and Viard, P. (2015) Ubiquitin-specific protease USP2–45 acts as a molecular switch to promote α2δ1-induced downregulation of Cav1.2 channels. *Pflugers Arch.* **467,** 1919–1929
71. Suzuki, S., Shuto, T., Sato, T., Kaneko, M., Takada, T., Suico, M. A., Cyr, D. M., Suzuki, H., and Kai, H. (2014) Inhibition of post-translational *N*-glycosylation by HRD1 that controls the fate of ABCG5/8 transporter. *Sci. Rep.* **4,** 4258

72. Comyn, S. A., Chan, G. T., and Mayor, T. (2014) False start: cotranslational protein ubiquitination and cytosolic protein quality control. *J. Proteomics* **100,** 92–101
73. Winchester, B. (2005) Lysosomal metabolism of glycoproteins. *Glycobiology* **15,** 1R-15R
74. Nakagawa, H., Wakabayashi-Nakao, K., Tamura, A., Toyoda, Y., Koshiba, S., and Ishikawa, T. (2009) Disruption of *N*-linked glycosylation enhances ubiquitin-mediated proteasomal degradation of the human ATP-binding cassette transporter ABCG2. *FEBS J.* **276,** 7237–7252
75. Hebert, D. N., and Molinari, M. (2012) Flagging and docking: dual roles for *N*-glycans in protein quality control and cellular proteostasis. *Trends Biochem. Sci.* **37,** 404–410
76. Cassidy, J. S., Ferron, L., Kadurin, I., Pratt, W. S., and Dolphin, A. C. (2014) Functional exofacially tagged N-type calcium channels elucidate the interaction with auxiliary $\alpha2\delta1$ subunits. *Proc. Natl. Acad. Sci. U.S.A.* **111,** 8979–8984
77. Cantí, C., Nieto-Rostro, M., Foucault, I., Heblich, F., Wratten, J., Richards, M. W., Hendrich, J., Douglas, L., Page, K. M., Davies, A., and Dolphin, A. C. (2005) The metal-ion-dependent adhesion site in the Von Willebrand factor-A domain of $\alpha2\delta$ subunits is key to trafficking voltage-gated Ca^{2+} channels. *Proc. Natl. Acad. Sci. U.S.A.* **102,** 11230–11235
78. Gee, N. S., Brown, J. P., Dissanayake, V. U., Offord, J., Thurlow, R., and Woodruff, G. N. (1996) The novel anticonvulsant drug, gabapentin (Neurontin), binds to the $\alpha2\delta$ subunit of a calcium channel. *J. Biol. Chem.* **271,** 5768–5776
79. Hendrich, J., Van Minh, A. T., Heblich, F., Nieto-Rostro, M., Watschinger, K., Striessnig, J., Wratten, J., Davies, A., and Dolphin, A. C. (2008) Pharmacological disruption of calcium channel trafficking by the $\alpha2\delta$ ligand gabapentin. *Proc. Natl. Acad. Sci. U.S.A.* **105,** 3628–3633
80. Song, L., Espinoza-Fuenzalida, I. A., Etheridge, S., Jones, O. T., and Fitzgerald, E. M. (2015) The R-domain: identification of an N-terminal region of the $\alpha2\delta$-1 subunit which is necessary and sufficient for its effects on Cav2.2 calcium currents. *Curr. Mol. Pharmacol.* **8,** 169–179
81. Ruscic, K. J., Miceli, F., Villalba-Galea, C. A., Dai, H., Mishina, Y., Bezanilla, F., and Goldstein, S. A. (2013) IKs channels open slowly because KCNE1 accessory subunits slow the movement of S4 voltage sensors in KCNQ1 pore-forming subunits. *Proc. Natl. Acad. Sci. U.S.A.* **110,** E559-E566
82. Berrou, L., Klein, H., Bernatchez, G., and Parent, L. (2002) A specific tryptophan in the I-II linker is a key determinant of β-subunit binding and modulation in CaV2.3 calcium channels. *Biophys. J* **83,** 1429–1442
83. Berrou, L., Dodier, Y., Raybaud, A., Tousignant, A., Dafi, O., Pelletier, J. N., and Parent, L. (2005) The C-terminal residues in the α-interacting domain (AID) helix anchor CaV β subunit interaction and modulation of CaV2.3 channels. *J. Biol. Chem.* **280,** 494–505
84. Buraei, Z., and Yang, J. (2013) Structure and function of the β subunit of voltage-gated calcium channels. *Biochim. Biophys. Acta.* **1828,** 1530–1540
85. Plant, L. D., Xiong, D., Dai, H., and Goldstein, S. A. (2014) Individual IKs channels at the surface of mammalian cells contain two KCNE1 accessory subunits. *Proc. Natl. Acad. Sci. U.S.A.* **111,** E1438–E1446
86. Burashnikov, E., Pfeiffer, R., Barajas-Martinez, H., Delpón, E., Hu, D., Desai, M., Borggrefe, M., Häissaguerre, M., Kanter, R., Pollevick, G. D., Guerchicoff, A., Laiño, R., Marieb, M., Nademanee, K., Nam, G. B., *et al.* (2010) Mutations in the cardiac L-type calcium channel associated with inherited J-wave syndromes and sudden cardiac death. *Heart Rhythm.* **7,** 1872–1882
87. Antzelevitch, C., Pollevick, G. D., Cordeiro, J. M., Casis, O., Sanguinetti, M. C., Aizawa, Y., Guerchicoff, A., Pfeiffer, R., Oliva, A., Wollnik, B., Gelber, P., Bonaros, E. P., Jr., Burashnikov, E., Wu, Y., Sargent, J. D., *et al.* (2007) Loss-of-function mutations in the cardiac calcium channel underlie a new clinical entity characterized by ST-segment elevation, short QT intervals, and sudden cardiac death. *Circulation* **115,** 442–449
88. Templin, C., Ghadri, J. R., Rougier, J. S., Baumer, A., Kaplan, V., Albesa, M., Sticht, H., Rauch, A., Puleo, C., Hu, D., Barajas-Martinez, H., Antzelevitch, C., Lüscher, T. F., Abriel, H., and Duru, F. (2011) Identification of a novel loss-of-function calcium channel gene mutation in short QT syndrome (SQTS6). *Eur. Heart J.* **32,** 1077–1088
89. Wormald, M. R., and Dwek, R. A. (1999) Glycoproteins: glycan presentation and protein-fold stability. *Structure* **7,** R155–R160
90. Zhao, Y., Sato, Y., Isaji, T., Fukuda, T., Matsumoto, A., Miyoshi, E., Gu, J., and Taniguchi, N. (2008) Branched *N*-glycans regulate the biological functions of integrins and cadherins. *FEBS J.* **275,** 1939–1948
91. Nagae, M., and Yamaguchi, Y. (2012) Function and 3D structure of the *N*-glycans on glycoproteins. *Int. J. Mol. Sci.* **13,** 8398–8429
92. Pertusa, M., Madrid, R., Morenilla-Palao, C., Belmonte, C., and Viana, F. (2012) *N*-Glycosylation of TRPM8 ion channels modulates temperature sensitivity of cold thermoreceptor neurons. *J. Biol. Chem.* **287,** 18218–18229
93. Watanabe, I., Wang, H. G., Sutachan, J. J., Zhu, J., Recio-Pinto, E., and Thornhill, W. B. (2003) Glycosylation affects rat Kv1.1 potassium channel gating by a combined surface potential and cooperative subunit interaction mechanism. *J. Physiol.* **550,** 51–66
94. Ohtsubo, K., and Marth, J. D. (2006) Glycosylation in cellular mechanisms of health and disease. *Cell* **126,** 855–867
95. Brundel, B. J., van Gelder, I. C., Henning, R. H., Tuinenburg, A. E., Deelman, L. E., Tieleman, R. G., Grandjean, J. G., van Gilst, W. H., and Crijns, H. J. (1999) Gene expression of proteins influencing the calcium homeostasis in patients with persistent and paroxysmal atrial fibrillation. *Cardiovasc. Res.* **42,** 443–454